NAVAL POSTGRADUATE SCHOOL

MONTEREY, CALIFORNIA

THESIS

TRANSIENT DYNAMIC RESPONSE AND FAILURE OF COMPOSITE STRUCTURE UNDER CYCLIC LOADING WITH FLUID STRUCTURE INTERACTION

by

Hui Fen Teo

September 2014

Thesis Advisor: Young Kwon
Second Reader: Jarema M. Didoszak

Approved for public release; distribution is unlimited

THIS PAGE INTENTIONALLY LEFT BLANK

REPORT DOCUMENTATION PAGE

Form Approved OMB No. 0704–0188

1. AGENCY USE ONLY *(Leave blank)*	**2. REPORT DATE** September 2014	**3. REPORT TYPE AND DATES COVERED** Master's Thesis

4. TITLE AND SUBTITLE
TRANSIENT DYNAMIC RESPONSE AND FAILURE OF COMPOSITE STRUCTURE UNDER CYCLIC LOADING WITH FLUID STRUCTURE INTERACTION

5. FUNDING NUMBERS

6. AUTHOR(S) Hui Fen Teo

7. PERFORMING ORGANIZATION NAME(S) AND ADDRESS(ES)
Naval Postgraduate School
Monterey, CA 93943-5000

8. PERFORMING ORGANIZATION REPORT NUMBER

9. SPONSORING /MONITORING AGENCY NAME(S) AND ADDRESS(ES)
N/A

10. SPONSORING/MONITORING AGENCY REPORT NUMBER

11. SUPPLEMENTARY NOTES The views expressed in this thesis are those of the author and do not reflect the official policy or position of the Department of Defense or the U.S. Government. IRB Protocol number ____N/A____.

12a. DISTRIBUTION / AVAILABILITY STATEMENT
Approved for public release; distribution is unlimited

12b. DISTRIBUTION CODE

13. ABSTRACT (maximum 200words)

With the growing interest in using composites in naval shipbuilding, it is crucial to understand the behavior of structures, especially the Fluid Structural Interaction (FSI) aspect of the composites under dynamic loading, to ensure the survivability of the platform at sea. The objective of this study is to perform displacement-controlled fatigue cyclic loading on quasi-isotropic E-glass laminate, which is commonly used in the shipbuilding industry. The fatigue cyclic loading is performed in both air and water environments with varied frequencies to analyze the structural behavior and failure pattern of composites under FSI.

The results of the experiment show significant FSI effects on the fatigue failure life cycle of the composite under high frequency loading of 2 Hz, 5 Hz and 10 Hz. The degree of FSI effect of the 5 Hz and 10 Hz cyclic loading is significantly higher than 2 Hz cyclic loading and the FSI effect varies for 5 Hz and 10 Hz, with 5 Hz loading exhibiting a higher impact on the composite. The knowledge gained from the investigation will benefit ongoing research into understanding the dynamic response and failure mechanism of the composite structures under FSI. The insights and suggestions for follow-on studies will contribute to the development of future life prediction modeling or tools that will help to prevent premature failures in the design of composite vessel—particularly a naval ship—where survivability is vital.

14. SUBJECT TERMS
fluid structure interaction, composite structures shipbuilding, fatigue loading

15. NUMBER OF PAGES
85

16. PRICE CODE

17. SECURITY CLASSIFICATION OF REPORT	**18. SECURITY CLASSIFICATION OF THIS PAGE**	**19. SECURITY CLASSIFICATION OF ABSTRACT**	**20. LIMITATION OF ABSTRACT**
Unclassified	Unclassified	Unclassified	UU

NSN 7540–01-280-5500

Standard Form 298 (Rev. 2–89)
Prescribed by ANSI Std. 239–18

THIS PAGE INTENTIONALLY LEFT BLANK

Approved for public release; distribution is unlimited

TRANSIENT DYNAMIC RESPONSE AND FAILURE OF COMPOSITE STRUCTURE UNDER CYCLIC LOADING WITH FLUID STRUCTURE INTERACTION

Hui Fen Teo
Civilian, Singapore Technologies Marine
B.S., Nanyang Technological University, 2008

Submitted in partial fulfillment of the
requirements for the degree of

MASTER OF SCIENCE IN MECHANICAL ENGINEERING

from the

NAVAL POSTGRADUATE SCHOOL
September 2014

Author: Hui Fen Teo

Approved by: Young Kwon
Thesis Advisor

Jarema M. Didoszak
Second Reader

Garth V. Hobson
Chair, Department of Mechanical & Aerospace Engineering

THIS PAGE INTENTIONALLY LEFT BLANK

ABSTRACT

With the growing interest in using composites in naval shipbuilding, it is crucial to understand the behavior of structures, especially the Fluid Structural Interaction (FSI) aspect of the composites under dynamic loading, to ensure the survivability of the platform at sea. The objective of this study is to perform displacement-controlled fatigue cyclic loading on quasi-isotropic E-glass laminate, which is commonly used in the shipbuilding industry. The fatigue cyclic loading is performed in both air and water environments with varied frequencies to analyze the structural behavior and failure pattern of composites under FSI.

The results of the experiment show significant FSI effects on the fatigue failure life cycle of the composite under high frequency loading of 2 Hz, 5 Hz and 10 Hz. The degree of FSI effect of the 5 Hz and 10 Hz cyclic loading is significantly higher than 2 Hz cyclic loading and the FSI effect varies for 5 Hz and 10 Hz, with 5 Hz loading exhibiting a higher impact on the composite. The knowledge gained from the investigation will benefit ongoing research into understanding the dynamic response and failure mechanism of the composite structures under FSI. The insights and suggestions for follow-on studies will contribute to the development of future life prediction modeling or tools that will help to prevent premature failures in the design of composite vessel—particularly a naval ship—where survivability is vital.

THIS PAGE INTENTIONALLY LEFT BLANK

TABLE OF CONTENTS

LIST OF FIGURES

LIST OF TABLES

THIS PAGE INTENTIONALLY LEFT BLANK

ACKNOWLEDGMENTS

First and foremost, I would like to express my greatest appreciation to Professor Kwon for his guidance and pointers during the course of my research and studies. The learning journey has been fulfilling and fruitful for my future career ahead.

My special thanks to my company and colleagues who have encouraged and given me the learning opportunity to pursue my studies in the Naval Postgraduate School.

I would like to also extend my gratitude to my forever loving, caring, and supportive mother, who has given me encouragement in my times of need and patience to tolerate my whims and fancies.

Last but not least, I would like to use this opportunity to express my heartfelt gratitude to everyone who has supported me throughout the course of my studies.

THIS PAGE INTENTIONALLY LEFT BLANK

I. INTRODUCTION

A. BACKGROUND

Modern-day shipbuilding has been steering toward the use of composites instead of the traditional steel hull to meet the increasing design requirements in the defense industry. Due to designers' limited knowledge of composite manufacturing and its mechanical performance in the early years, naval composite vessels were limited to no more than 15 m in length and 20 tonnes displacement. Only in recent years the fabrication of larger ships such as the Visby Class Corvettes and Skjold-class corvettes was materialized with an optimized design, good material strength, and improved mechanical properties using low cost composites [1]. However, ships made entirely of composites of 100m in length and longer are still undergoing paper design and have not been manufactured as yet.

The corrosion resistance, electromagnetic absorption properties, and the significant weight savings of the composites provide potential growth and performance capabilities for future platforms. Renewed Interest in the exploration of using composite structures for naval shipbuilding were sparked after the first U.S. Navy DDG 1000 Zumwalt-class destroyer was contracted in February 2008 for US$6.3 billion. It consisted of a full composite superstructure with steel hull [2]. With the growing interest in using composites in naval shipbuilding, it is crucial to understand the behavior of these structures, especially the fluid structural interaction aspect of the composites under dynamic loading, to ensure the survivability of the platform at sea.

Figure 1. Picture of the Visby class and Skjold vessel (from [3], [4]).

B. RESEARCH EFFORTS

Previous research has highlighted the importance of fluid structure interaction (FSI) and how it lowers the natural frequency and influences modal shapes of structures. The effects of FSI primarily revolve around the theory that added mass causes structures to fail more rapidly in a submerged environment. Multiple experiments have been performed to verify the “added mass” theory and how the structure responds to dynamic loading in simulated sea-going conditions. This chapter looks into the cause of hydrodynamic mass effect, the structure’s reaction to low velocity cyclic loading, fatigue cycles, stress ratio, S-N curve, and moisture.

1. Hydrodynamic Added Mass Effect

Under a vibrating load in immersed conditions, the total kinetic energy of a structure increases due to the added kinetic energy from the water impacting the structure [5]. The inertial forces that result from the acceleration of the fluid impacting the structure create a virtual force known as the “added mass” effect. The increase in damping due to the “added mass” effect decreases the natural frequency and changes the dynamic response of a structure [6].

The degree of “added mass” effect is more detrimental to a composite structure than to the traditional steel hull. This is because, the ratio between water to composite density is higher than the ratio of water to steel density which results to a higher Non-dimensionalized Added Virtual Mass Incremental (NAVMI) facter, Γ, shown in Equation 1.2. The numerical formula for the NAVMI factor, Γ, is used to approximate the degree of difference between steel and

composite structures under fluid structure interaction on circular and rectangular plates [7].

$$f_w = \frac{f_a}{\sqrt{1+\beta\Gamma}} \tag{1.1}$$

$$\Gamma = \frac{\rho_w a}{\rho_p h} \tag{1.2}$$

where f_w and f_a are the natural frequency in water and air, ρ_w and ρ_p, represent the density of water and plate, and β is the non-dimensional correction factor. According to the published results from Kwah [7] and Owens [8], the NAVMI factor of a steel plate submerged in water ranges from 1.4 to 2.4 and these values depend on the boundary conditions of the experiment, such as the height of the submerged volume and the geometrical dimensions of the rectangular plates. Research done by Owens [8] also found that the NAVMI factor for a composite plate is at least 6.6, which is significantly higher than the added mass effort on steel. This result gave a quantitative comparison to affirm and reinforce the importance of understanding the FSI on composite and the degree of hydrodynamic “added mass” effect which impacts the structures while submerged.

2. Low Velocity Impact and Cyclic Loading

Dynamic loading on the ship hull structure is often categorized as impact/impulsive loading and vibratory loading, which comes in the form of random, transient, or steady state [9]. Low velocity impact loading is often induced by the constant slamming loads from the waves and the debris at sea in green water. Damage due to cyclic loading on composites is usually subtle as a crack propagates though the fiber layers within the composite. Signs of failure are usually visible after a prolonged period of numerous loading. As such, it is

vital to understand the failure response and the effect of FSI of the composite under vibration loading.

Under low velocity impact, composite structures experience an added mass effect which causes them to fail more rapidly in a submerged environment. Owens [8] found that the added mass effect due to FSI increased the force of impact by 50 percent and the strain exerted on a composite plate by 20 percent to 50 percent under low velocity impact. The natural frequency of the composite was also found to decrease by half when it was submerged in water. Research done by Violette [10] shows that composite structures in contact with water tend to exhibit a larger strain deformation compared to a dry baseline under low velocity impact. Furthermore, the delamination pattern of composite deformation propagates to a larger surface area in the submerged condition. Working upon the research done by Violette, Conner [11] affirms the results that the dynamic response of a composite structure in contact with water is significantly larger than a dry baseline and the added mass effect is not uniform throughout the surface of the composite panel.

Priest [12] has done a series of experiments comparing the free vibration response of a composite structure under FSI and found that the natural frequency of the composite under submerged conditions decreased by one-third as compared to the natural frequency of the composite in air. Under free-free beam, the natural frequency of the composite was decreased by half with the added mass.

3. Fatigue Cyclic Test

There are numerous intensive studies in understanding the delamination and fatigue failure characteristics of composites. Having a good understanding of the loading conditions and the failure characteristics of the composite allows better prediction of the fatigue life of composites with respect to the anticipated loading.

Degriek and Van Paepegem [13] summarize the parameters that affect fatigue failure and these parameters involve the selection of fiber and matric types, reinforcement strictures (fabric, braiding, unidirectional), stacking sequence and orientation, environmental conditions (temperature and moisture), and loading conditions.

The loading conditions that affect fatigue failure highlighted by [13] involve the stress ratio R and cyclic frequency of the dynamic loading. In the review, they pointed out that the cyclic frequency and loading rate have considerable influence on the fatigue failure of composites due to the internal heat generation and the possible associated temperature increase.

a. Stress Ratio R

The stress ratio, R, is governed by the ratio of the minimum, $\sigma_{\min}$, and maximum, $\sigma_{\max}$, stress of the loading cycle under fatigue test.

$$R = \frac{\sigma_{\min}}{\sigma_{\max}} \tag{1.3}$$

The R-ratio has been frequently used as a parameter that largely influences the fatigue response of composites. Fatigue test results done by Cain et al. [14] on E-glass composite laminate has shown quantitative and qualitative differences in both the life cycle and failure pattern for R-Ratio of values R=0.1 (tension tension), R = -1 (tension compression), and R=10 (compression compression). Fatigue tests performed by Gaprino on glass fiber composite show that compressive cycle loading of R=1.43 has a longer life cycle when compared to R=10 and the stress ratio R has a strong influence on fatigue life [15].

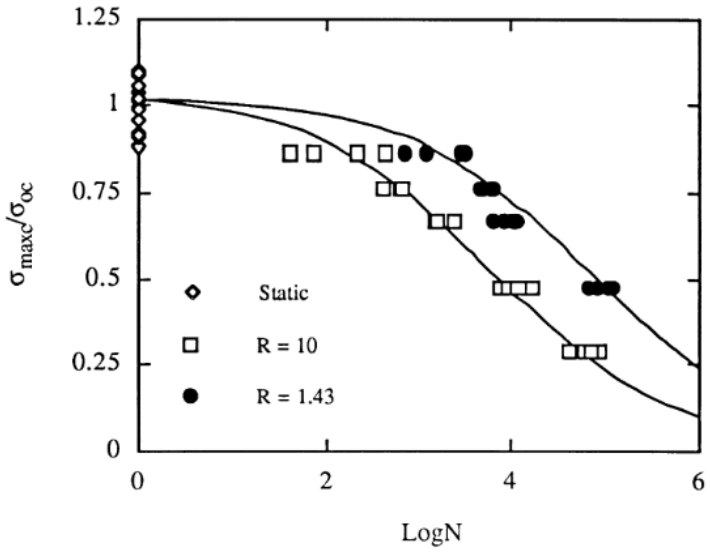

Figure 2. Semi-log plot of the non-dimensional maximum applied stress against number of cycles to failure (from [15]).

b. S-N Curve

The degradation of a composite undergoing cyclic loading generally exhibits a different stage of damage loading which involves matrix cracking through the fiber-matrix interface, followed by fiber-matrix debonding, fiber breakage, and delamination between the composite layers. The microcracks on the surface of damage impact are described to distribute the stress concentration and increase the residual strength of the composite [16]. In most of the research, the classic S-N curve has been used to correlate the fatigue life cycle failure of composites.

Khelifa and Al-Shukri discuss the fatigue-life diagram using the S-N curve. He has divided the characteristics and type of damage mechanism of glass polyster composites into three regions in a S-N curve. Region I shows scattered data with static critical stress to failure. The failure mechanism is due to a large volume of debonding across the composite. Region II is described as the progressive damage region with life cycles above $5x10^4$ cycles. The damage progression rate increases proportionally with the loading rate of the composite.

Region III shows that the stress is insufficient to inflict any damage to the composite and the fatigue life cycle goes beyond 10^6 cycles [17].

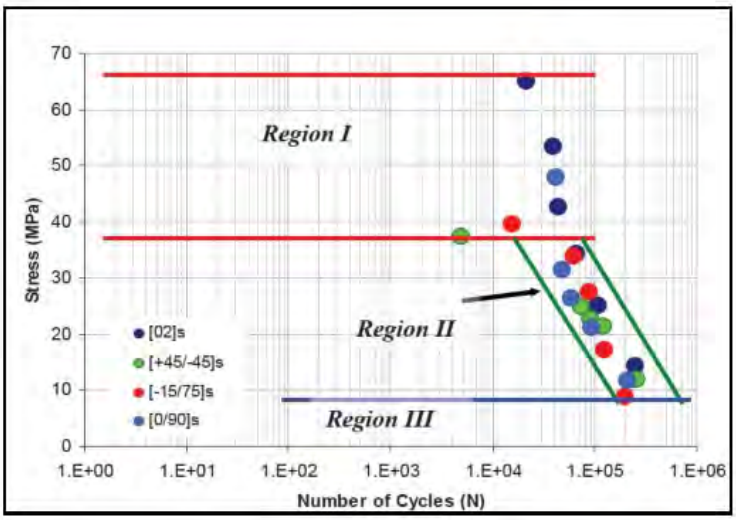

Figure 3. The Fatigue Life Diagram (from [16]).

c. Moisture

Porter has experimentally evaluated the effects of moisture and temperature on the structural integrity of composite laminates which are flawed. Static and cyclic loading tests were performed on composite specimens with slits of varied sizes under dry and moist conditions. The moist condition for the wet specimen was prepared by soaking the specimen in water for eight weeks with a weight gain of 1.3 percent to 1.5 percent. The loads are applied perpendicular to the slit. Under static tension and compression loading for dry and wet specimens in varied temperature, the author has found the deflect size of the slit degrades more significantly with varied temperature for the wet specimen as shown in Figure 4. The author also indicates that the fatigue test results for the tension-compression loading (R= -1) for the wet specimen degrades more significantly at the initial life cycles shown in Figure 5 [18].

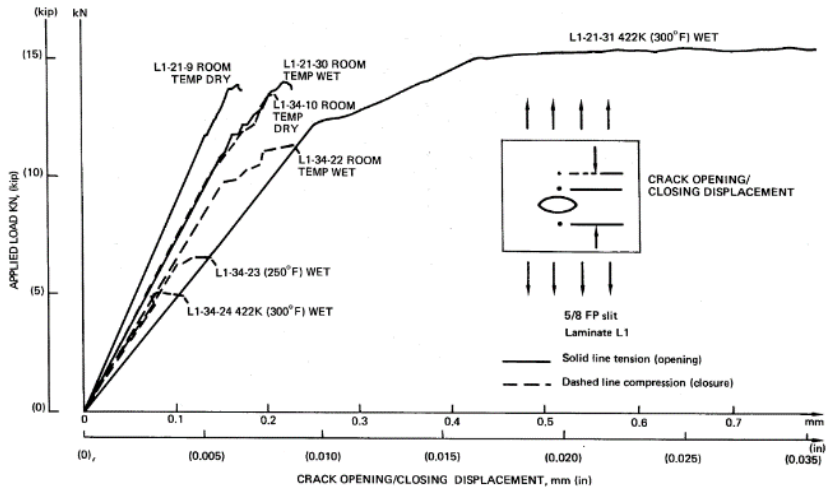

Figure 4. Typical crack opening/closing displacement records for test specimen (from [18]).

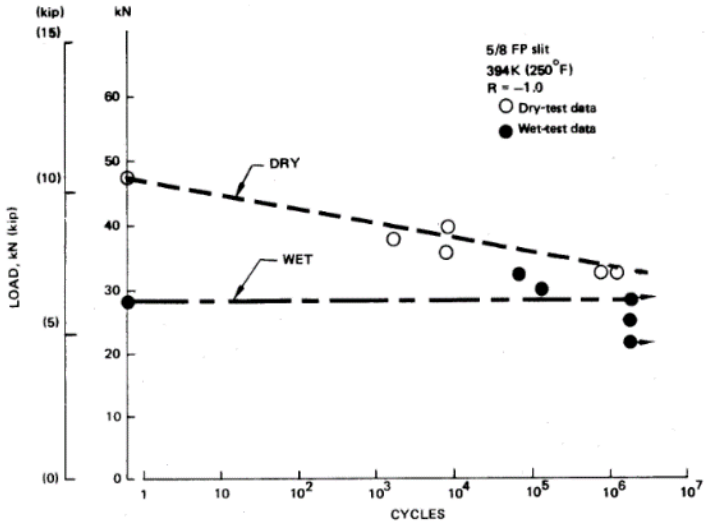

Figure 5. Fatigue test data for 5/8” slit specimen at 394K (from [18]).

A review of the current research on the effect of FSI on composites gives insight and motivation for understanding the effects of fluid structure interaction under cyclic loading. Sea going vessels are constantly being subjected to cyclic vibrations from the machineries onboard and the slamming impact from the sea waves. Little has been uncovered, though, to investigate the response of transient cyclic loading on composites and the possible response of and the

failure rate from the composite. Although there are numerous studies on fatigue failure and structural integrality of composites under cyclic loading, most of the experiments performed are uniaxial stress conditions which are rarely applicable to real structures [13].

Degriek and VanPaepegem [13] highlighted the difficulty of understanding fatigue failure was due to the complex structural component of composites and the difficulty of fabricating identical composites during experimental testing.

C. OBJECTIVE

This study focuses on performing displacement controlled fatigue cyclic loading on quasi-isotropic E-glass laminate, which is commonly used in the shipbuilding industry. The experimental work is performed in both the air and water submerged environment to simulate sea going conditions and for analysis of the structural behavior and failure pattern of composites under FSI. The knowledge gained from the investigation will benefit ongoing research into understanding the dynamic response and failure mechanism of the composite structures under FSI. The insights and suggested follow-on studies can contribute to the development of future life prediction modeling or tools which will help to prevent any premature failure in the design of a vessel—particularly, a naval ship, where survivability is vital.

THIS PAGE INTENTIONALLY LEFT BLANK

II. COMPOSITE FABRICATION

A. COMPOSITE SELECTION

Composites are materials that are formed by combining two or more materials of different physical and chemical properties [19]. The fiber fabric and resins are usually the two main materials that form an advanced fiber-reinforced composite material. The strength and stiffness of the composite are usually derived from the type of woven fiber reinforcements chosen and the number of layers used to fabricate the composite. Figure 6 shows the different types of fibers and their corresponding specific strength.

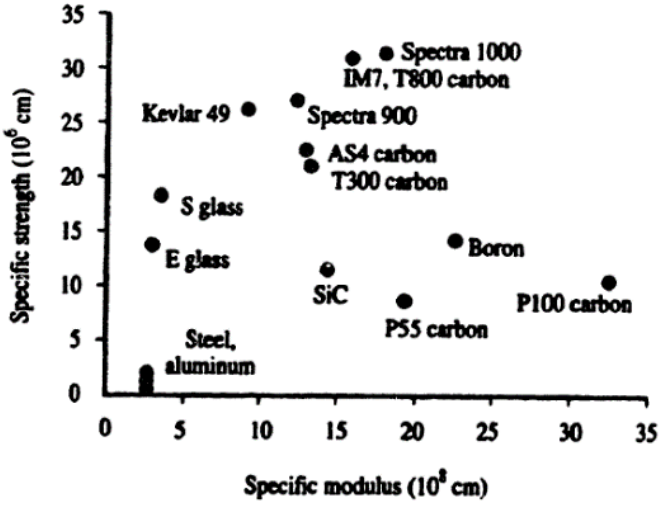

Figure 6. Specific modulus and specific strength of the various engineering materials and fibers (from [20]).

1. E-glass Fiber

There are many types of fibers that are generally used in marine structures, but among them all, E-glass fiber is most commonly used in shipbuilding for massive ship structures such as ship hulls and ship superstructures. Being lightweight, cost effective, and resistant to moisture seepage, E-glass is a more commercially viable solution for shipbuilding and

repair. Figure 7 shows the list raw fiber properties compared to the cost of the materials. Many prior experiments and research have been performed using E-glass fiber as the test specimen. Thus, there are many available resources and data that can be consulted when selecting E-glass as the test specimen [21].

Fiber	Tensile Strength ($psix10^3$)	Tensile Modulus ($psix10^3$)	Ultimate Elongation	Cost, US $/lb (2001)	Cost, US $/lb (1994)
E-glass	500	10.5	4.8%	0.92-2.00	0.8-1.2
S-glass	665	12.6	5.7%	6-10	4
Kevlar®	525	18	2.9%	14-20	16
Spectra® 900	375	17	3.5%	NA	22
Carbon	350-700	33-57	0.38-2.0%	8-30	17-450

Figure 7. Raw fiber properties (from [21]).

The motivation of this study is to identify the failure pattern and the dynamic response of the composite under fluid structure interaction applied in the marine industry. Since E-glass is generally used for ship construction and there have been prior experimental and research efforts done using E-glass fibers, E-glass is selected for this thesis (Figure 8).

Figure 8. E-glass woven fabric.

2. Epoxy Resin

The selection of polymer matrix resin for E-glass reinforced fiber has to take into account curing time and temperature, ease of handling, and physical properties of the resin. In this study, epoxy resins are selected due to their high strength, the stiffness of the material, and their compatibility with the workshop manufacturing process which will be elaborated in the next section. The resin and hardener used are M1002 Resin with Pro-Set 237 hardener, and the epoxy is mixed in a ratio of 100:28, according to the recommendation from the supplier.

Figure 9. Epoxy resins.

B. FABRICATION PROCEDURE

There are numerous ways to fabricate composites on a small scale, and since the objective of the thesis is to fabricate a small quantity of composites for testing, the molding facility has to be cost effective and easily set up in a laboratory while minimizing safety hazards. The fabrication method chosen is to perform “wet layup” of the composite laminates, followed by Vacuum Assisted Resin Transfer Molding (VARTM).

1. Wet Layup

“Wet layup” is a basic fabrication method that consists of layering the dry E-glass woven fabric with the epoxy resins. The epoxy resins are spread evenly onto each layer of E-glass woven fabric fibers using a hand roller, and each ply of the fabric is evenly coated with the resins [22].

The number of layers of the composite fabric determines the strength and stiffness of the composite. For the experiment, 23 layers of E-Glass woven fabric are used to fabricate a composite panel measuring 21 inches long by 16 inches wide. To form the epoxy resin, 250 ml of Pro-Set M1002 Resin is gently mixed with 83 ml of Pro-Set 237 hardener at room temperature. According to the manufacturer’s directions, the hardener will take 4.5 hours to 6 hours of open time before the epoxy starts to harden. It is preferred to complete the wet layup within 3 hours before the epoxy resin starts to thicken and cure [23].

The laminated composite will then go through VARTM to extract the excess epoxy and any trapped air pockets before curing takes place. Figure 10 shows the process of layering the composite and the laminated composites before VARTM.

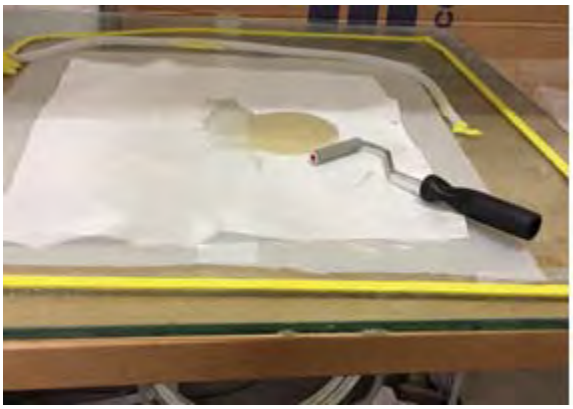

Figure 10. Wet layup procedure.

2. Vacuum Assisted Resin Transfer Molding (VARTM)

Fabrication of composites using VARTM is a low pressure manufacturing process that is cost effective; it does not require any expensive equipment to maintain the environment of high heat or high pressure. The VARTM uses low pressure to draw out excess resins and trapped air pockets from the composite into a bleeder cloth by vacuum. The bleeder cloth will absorb the excess resins from the composite laminate and provide a constant air path for the vacuum to minimize trapped air at the surface of the laminate [24].

The materials required for VARTM, shown in Figure 11, are as follows:

- Teflon Sheet–Placed at the bottom of the composite laminate.
- Perforated Ply–Placed after the composite is laminated. It is used to separate the bleeder cloth and the composite laminate. The perforated holes allow the resins to bleed out.
- Bleeder cloth–A layer of white cloth that absorbs excess resins and creates a vacuum air path to prevent trapped air at the surface of the laminate.
- Plastic Film–Acts as a vacuum bag to contain or prevent air leakage.
- Sealant Tape–Seals the plastic film and creates a vacuum environment.

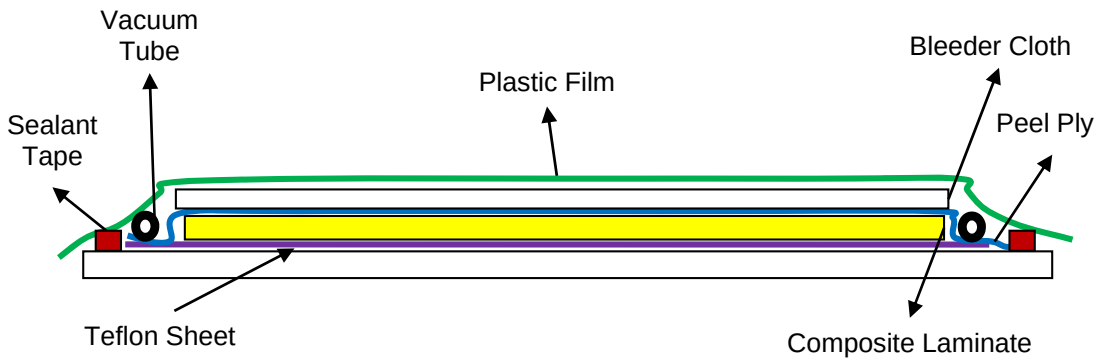

Figure 11. Diagram of VARTM fabrication.

Before the VARTM process starts, the laminated composite is first layered with the perforator ply followed by the bleeder cloth to remove excess resin and air pockets on the surface of the laminate. The laminated composite is then covered with a plastic film and placed over the top of the sealant tape to form a vacuum-tight seal. Once the vacuum pump is activated, the vacuum seals the composite laminate and keeps it at 103.4 kPa (15 psi) for the duration of 24 hours for the composite to cure. Figure 12 shows a composite laminate panel made under the VARTM process.

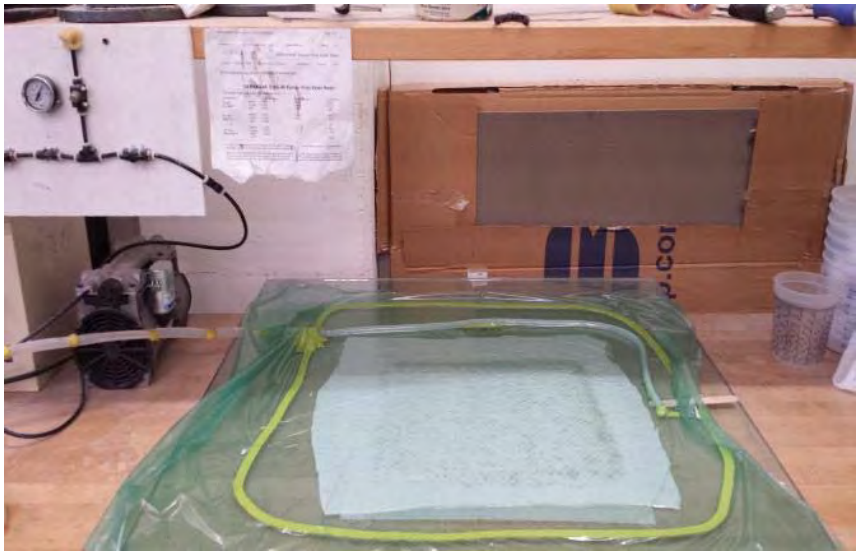

Figure 12. VARTM and composite panel being made.

3. Composite Panels

After 24 hours of curing, the composite panel is cut into 20 pieces of test samples for the experiment. Each sample is cut into rectangular strips measuring 0.23 meters (9 in) in length by 0.038 meters (1.5 in) in width for cyclic loading testing. The diagram in Figure 13 shows the cutout from the composite panel and Figure 14 shows the composite panel after 24 hours of curing.

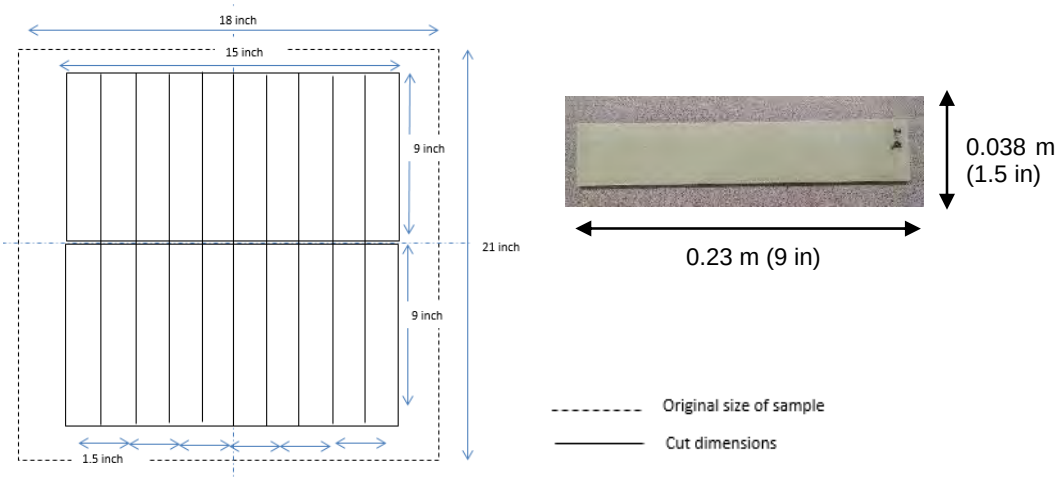

Figure 13. Cutout dimensions of the test sample.

Figure 14. Composite panel after curing.

THIS PAGE INTENTIONALLY LEFT BLANK

III. EXPERIMENT METHODOLOGY

The objective of the experiment is to perform fatigue cyclic loading on the composite samples in air and in water submerged conditions. The results derived from the experiment will be used as the basis to analyze the effects of FSI on composites and how the failure pattern will be affected by varying the frequency of the cyclic loading.

To determine the loading condition for the cyclic loading experiment, a three point bending test is first performed to identify the stress strain characteristic and maximum yield strength of the composite. After that, the experiment proceeds with fatigue cyclic test of the test samples in air and water submerged environments. To perform the experiment, the following equipment and apparatuses are used.

A. EQUIPMENT USED

Both the three point bending test and fatigue cyclic test use the Material Testing System (MTS) machine to determine the mechanical strength and fatigue life cycle of the composite.

1. Material Testing System (MTS 858)

The MTS machine is a multipurpose servo-hydraulic testing system designed for dynamic and static loading. It is equipped with force transducers and load control modules that detect and exert precise static and dynamic loading. The MTS machine and its specifications are summarized in Figure 15 and Table 1 respectively.

Table 1. MTS 858 specifications (after [25]).

Description	Performance
Force Range	1 kN – 500 kN
Range of performance	Moderate
Testing Materials	Usually lower strength materials ranging from plastics, elastomers to aluminum
Specimen Size	Small and Sub-sized
Frequency Range	1 Hz to 10 Hz
Capability Performance	Monotonic Test (Tension, compression, and bending), Fatigue Test, Fracture Testing, Component Testing, *High Temperature Testing, *Biomedical Testing, *Thermal Mechanical Fatigue Testing, *Axial Torsion Testing, *Planar Biaxial Testing, and *High Force Testing
Basic Test Ware Software	Controls the setup of the MTS to perform monotonic and cyclic loading test by defining the inputs of the frequency, amplitude, and force or displacement control. Data capturing is enabled while the experiment is running in real time and data can be easily exported to word processing software.

*Capabilities can be performed only if the required add-on equipment/loading jig is purchased.

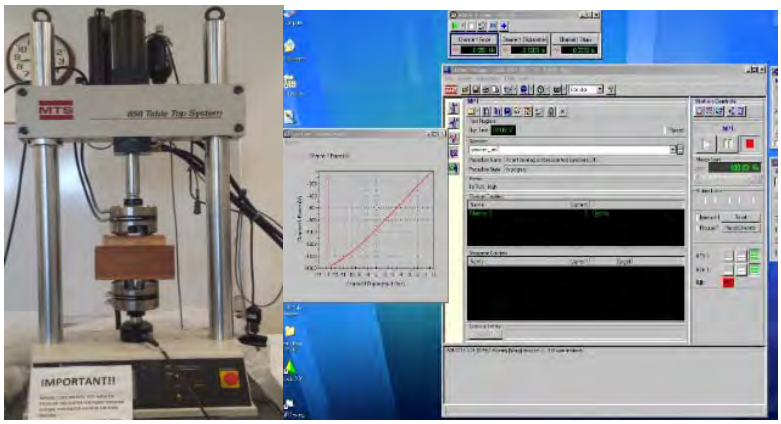

Figure 15. MTS machine and the software mimics.

2. Loading Jig

To position the test sample onto the MTS Machine for cyclic loading test, a loading jig is used. It holds the specimen in place as shown in Figure 16. To prevent slippage during the experiment, the ends of the specimen are loosely secured with Velcro strips onto the loading jig.

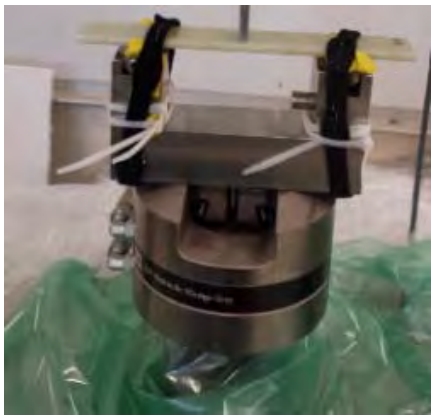

Figure 16. Loading jig.

3. Water Tank

As the experiments will be performed in water submerged conditions, a water tank is required to hold the sample and the loading jig during the cyclic loading test. A water tank made of acrylic, shown in Figure 17, is used for this purpose.

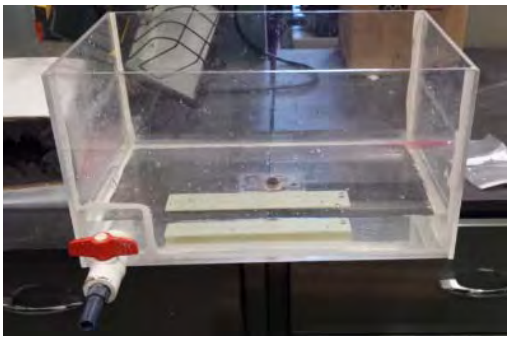

Figure 17. Water tank.

B. THREE POINT BENDING TEST

As strength of the composite depends on many variable factors such as the fiber stacking layers, orientation, and fabrication methods, it is important to perform a three point bending test to determine the stress strain characteristic of the composite fabricated. The three point bending test is performed for every batch of composite panel and the values of the maximum force and displacement are used to determine the loading condition for the fatigue cyclic loading test.

1. Test Procedure

To set up the experiment, the sample is loosely secured to the loading jig to prevent any slippage during the test. The loading jig is subsequently clamped onto the MTS Machine with the load cell aligned to the center of the composite in preparation for the three point bending test shown in Figure 18.

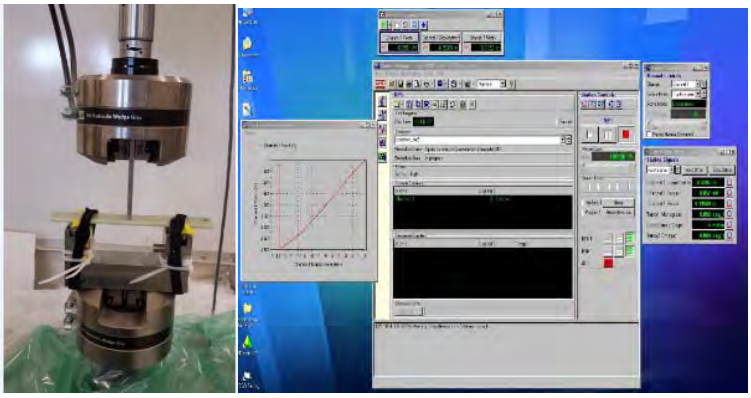

Figure 18. Three-point bending test on MTS Machine.

2. Data Acquisition

Using the built-in software that comes with the MTS Machine, the strain rate and the data acquisition of the experiment can be controlled. The Basic Test Ware software was programmed to record the force reading from the transducer at the period of 0.05 seconds per data point and to control the strain rate of the load cell at 2 mm/min. The software plots and displays the force displacement

curve of the three point bending test in real time while the experiment is still running.

Data captured from software shows the force displacement curve of the composite during the three point bending test. The ultimate yield strength of the composite can be easily identified from the graph when a sharp decrease in force is observed. This signifies the delamination of the composite and crack propagation through the adhesive bond layers which cause the specimen to fail. The results from the three point bending test are used to determine the natural frequency of the composite sample and the loading condition for the subsequent experiment for the fatigue cyclic test.

The fatigue cyclic loading test will be conducted in both air and water submerged conditions to identify the possible pattern in fatigue failure and investigate the influence of FSI on composites. The fatigue cyclic experiment will be performed in the laboratory using the MTS Machine to perform the cyclic loading. The experiment will also vary the frequency of the loading to investigate its relationship to the failure pattern.

3. Loading Conditions

Using the results from the three point bending test, the load ratio of the compressive fatigue cycle is R=3, where R is the ratio of the maximum and minimum displacement of the composite fixed at 75 percent and 25 percent, respectively. The sinusoidal frequency for the compressive cyclic fatigue test is varied at 10 Hz, 5 Hz and 2 Hz in air and water submerged environment. The Target Set Point and Amplitude are calculated based on the formula shown in Figure 19. The loading condition is keyed into Basic Test Ware to control the cyclic loading of the machine.

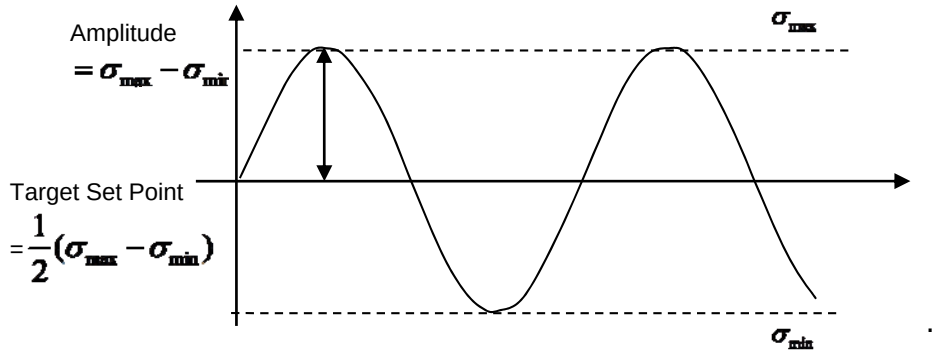

Figure 19. Frequency of load.

4. Test Procedure for Fatigue Cyclic Loading

The testing principles for the cyclic loading on air and on water submerged environment are the same. However, to create the water submerged condition for the composite sample, a half-filled water tank is used in the experiment.

a. Cyclic Loading in Air

Similar to the three point bending test, the composite sample is secured to the loading jig, which is mounted onto the MTS Machine. Since the specimen will be undergoing high frequency cyclic loading, it is important to gently secure the sample to prevent any possible slippage during the experiment. The input parameters of the loading condition include the frequency, amplitude, target set point, and data acquisition rate for the fatigue cyclic test shown in Figure 20. After the values are keyed into the Basic Test Ware, the hydraulic servo motor and actuating system exert a displacement controlled cyclic loading onto the composite sample.

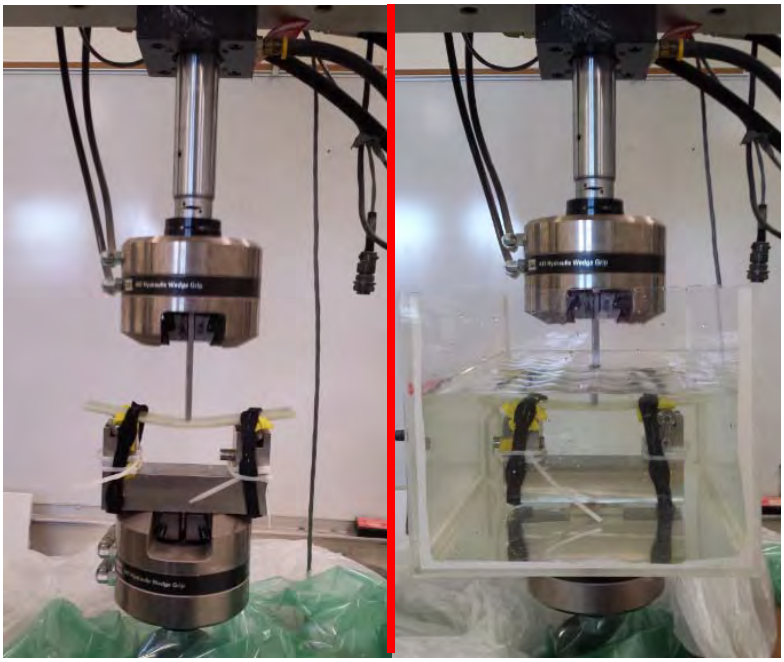

Figure 20. Cyclic loading in air and water submerged environment.

b. Cyclic Loading in Water Submerged Condition

To perform the experiment, the water tank is first mounted onto the MTS Machine. The loading jig holding the composite specimen is then fixed to the bottom of the water tank for testing. To ensure consistency in the results, the water is constantly filled to three-quarters full during the water submerged fatigue test. Figure 21 shows the setup of the experiment with the composite sample submerged in water.

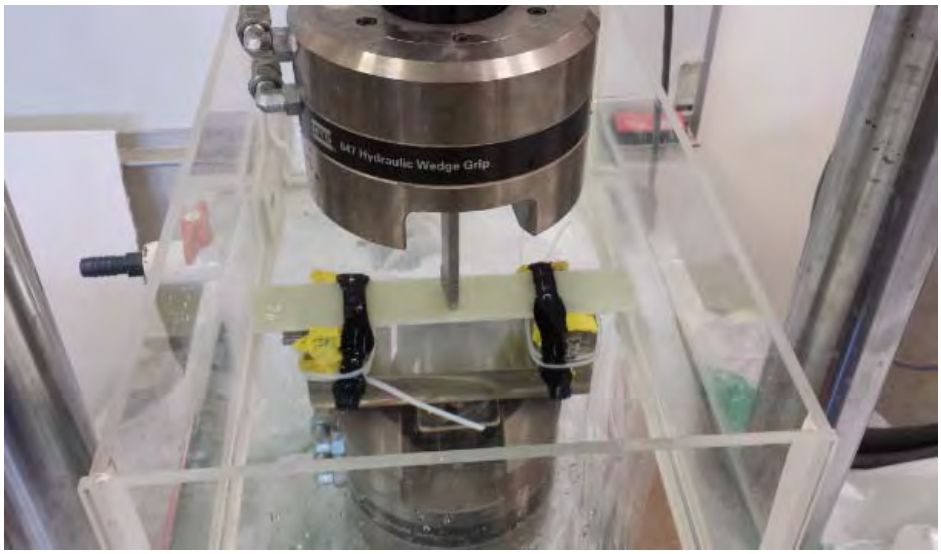

Figure 21. Setup for cyclic loading in water submerged condition.

5. Data Analysis

The output of the data files from the Basic Test Ware shows the transient response of the sample with force and displacement as a function of time. With a data acquisition rate of 0.025 seconds/data, we are able to observe the periodic response of the composite sample under constant displacement-controlled cyclic loading. The cyclic loading on the sample is tested to failure. Depending on the duration of the experiment, the data files populated by the software will be large and a MATLAB program has to be written to filter out the unnecessary data points collected.

IV. ANALYSIS OF RESULTS

In this research, a total of five sets of test samples were chosen for this analysis. To ensure that all composites have the same baseline for the comparison study, the materials, manufacturing process, and dimensions of the samples were all kept constant. Twenty samples were cut from each batch of composites fabricated to perform the three point bending test and fatigue cyclic loading test. The initial experiment was to perform a cyclic loading test of 10 Hz but the scope of study has progressively expanded to perform cyclic loading for 5 Hz and 2 Hz for both air and water submerged conditions.

A. THREE POINT BENDING TEST RESULTS

This section analyzes the results of the three point bending test, which was performed to determine the mechanical properties of the composite fabricated, as well as to determine the loading conditions for the subsequent fatigue cyclic loading experiment. In addition, this section examines the importance of determining the natural frequency of the composite sample to ensure that it does not coincide with the loading condition of the fatigue cyclic loading experiment.

1. Mechanical Properties of Composite

The three point bending test was performed to determine the mechanical properties of the composite fabricated. Although all the composites are fabricated using the same baseline, the maximum force and displacement of the composites still varies. Table 2 shows the mechanical properties of all the composites fabricated.

Table 2. Mechanical properties of composites fabricated.

*Batch	2	3	4	5	6
Thickness (mm)					5
Max Strength (N)	1777	1431	1573	1536	1548
Max Displacement (mm)	13.4	15.9	12.7	14.0	12.4
Stiffness (kN/m)	142.8	97.8	135.8	122.9	138.1

*Batch 1 of the composite fabricated was not included in the experiment data due to the difference in loading condition from the rest of the specimens.

The Figure 22 shows the force displacement curve of the composite samples under the three point bending test. All the composites exhibit an initial nonlinear and inelastic deformation trend and end with a catastrophic abrupt failure. The disparity of the failure strength among the composite samples can be due to the duration and initial learning curve of fabricating composites during the wet layup process.

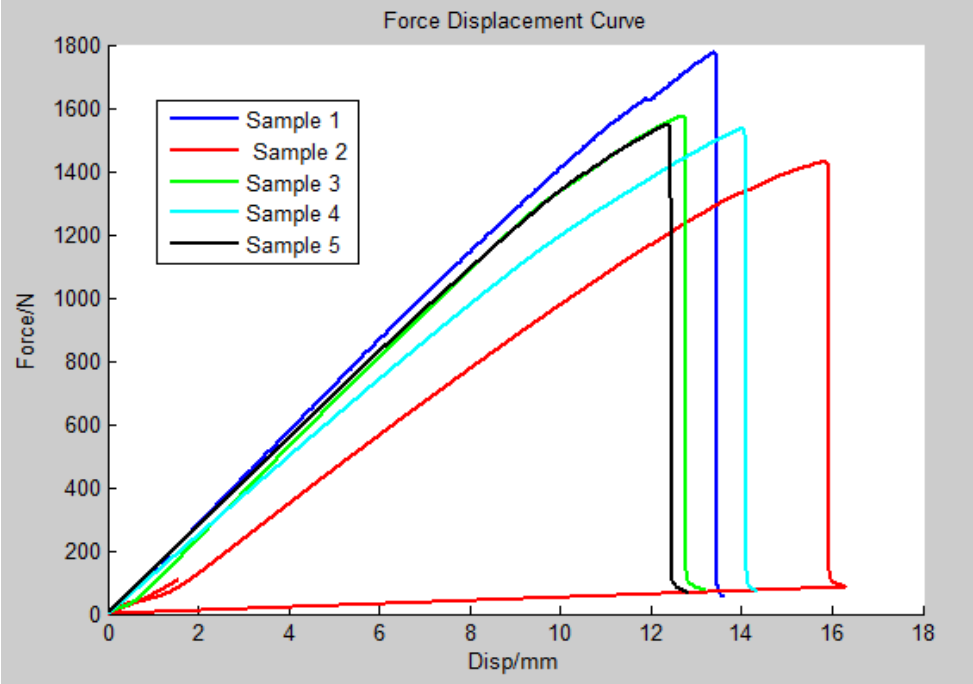

Figure 22. Graph of force displacement curve of all the composite samples.

The objective of performing the three point bending test is to determine the loading conditions for the subsequent fatigue cyclic loading experiment. Since the mechanical strength of the sample varies slightly among the batch of composites fabricated, the loading conditions were fixed at 75 percent and 25 percent of the maximum displacement of each set of composite samples. Table 3 shows the loading conditions of the fatigue cyclic loading test. The loading conditions are applied to the rest of the specimens cut out from each set of composites fabricated.

Table 3. Loading conditions for fatigue cyclic loading.

Set	Max Disp (mm)	Upper Cyclic Disp (mm)	Lower Cyclic Disp (mm)	Mean Cyclic Disp (mm)
2	13.4	10	3.35	6.68
3	15.9	12	4	8.00
4	12.7	9.6	3.2	6.40
5	14.0	10.5	3.5	7.00
6	12.4	9.3	3.1	6.20

2. Natural Frequency of Sample

To avoid resonance during the fatigue cyclic loading test, it is important to determine the natural frequency of the composite sample to ensure that it does not coincide with the loading condition of the experiment.

According to the Euler's equations, the natural frequencies of vibration for beam structure, ω_n can be computed using Equation (4.1), where l is the effective length, E is the elastic modulus, I is the second moment of area, ρ is the mass per unit length of the specimen, and β_n is the eigenvalue constant which depends on the boundary conditions of the problem. The value of $(\beta_n \ell)^2$ for fundamental vibration mode is 9.87 from Table 4, listing the typical end conditions of $(\beta_n \ell)^2$.

$$\omega_n = (\beta_n \ell)^2 \sqrt{\frac{EI}{\rho}} \tag{4.1}$$

Table 4. Numerical values of $(\beta_n \ell)^2$ for typical conditions (from [26]).

Beam Configuration	$(\beta_n \ell)^2$ Fundamental	$(\beta_n \ell)^2$ Second Mode	$(\beta_n \ell)^2$ Third Mode
Simply supported	9.87	39.5	88.9
Cantilever	3.52	22.0	61.7
Free-free	22.4	61.7	121.0
Clamped-clamped	22.4	61.7	121.0
Clamped-hinged	15.4	50.0	104.0
Hinged-free	0	15.4	50.0

To determine the elastic modulus and second moment of area, EI, of the specimen, the values can be computed from the force displacement curve generated from the results acquired from the three point bending test. According to the Euler–Bernoulli beam theory, the equation of deflection, δ, for a simply supported beam with point load at the middle and the equation of Beam Stiffness, k, is as shown in Equation (4.2) and Equation (4.3), respectively. The equation for EI can be derived in Equation (4.4) [26].

$$\delta = \frac{F\ell^3}{48EI} \tag{4.2}$$

$$k = \frac{F}{\delta} \tag{4.3}$$

$$EI = \frac{k\ell^3}{48} \tag{4.4}$$

Following the three point bending test, the physical parameters and the stiffness of the specimen were determined and are listed in Table 5. The natural frequency of each sample is calculated using Equation 4.1 and 4.5 are summarized in Table 6.

Table 5. Physical parameters of specimen.

Parameters	
Length (m)	0.23
Width (m)	0.039
Thickness (m)	0.005
Effective Length (m)	0.14
Mass per unit length, ρ (kg/m)	0.3139

Table 6. Natural frequency of all the composite samples.

Batch	**k (N/m)**	**EI**	ω_n **(rad/s)**	ω_n **(Hz)**
2	142800	8.1634	2567.98	408.65
3	97800	5.5909	2125.19	338.19
4	135800	7.7632	2504.25	398.51
5	122900	7.0258	2382.34	379.11
6	138100	7.8947	2525.37	401.87

The result in Table 6 tabulates the natural frequency of a simply supported composite beam structure in air. For the water submerged condition, literature reviews and numerical analysis suggest that the natural frequency of structure is reduced by approximately half when compared to air conditions [8].

Bearing in mind that the fatigue cyclic loading will be performed in both air and water submerged conditions, the natural frequency of the composite sample for both conditions is significantly higher than 10 Hz. As such, it is unlikely that resonance of vibration interfered with the results of the experiment.

B. FATIGUE CYCLIC LOADING

This section analyzes the results of the fatigue cyclic loading, which was performed to determine the life cycle of the composite sample in air and water submerged conditions under varied frequency cyclic loading of 10 Hz, 5 Hz and 2 Hz. This section will begin with the process of analyzing the data according to the data filtering algorithm shown in Figure 23 follow by the results of analyze for fatigue cyclic loading for 10 Hz, 5 Hz, and 2 Hz.

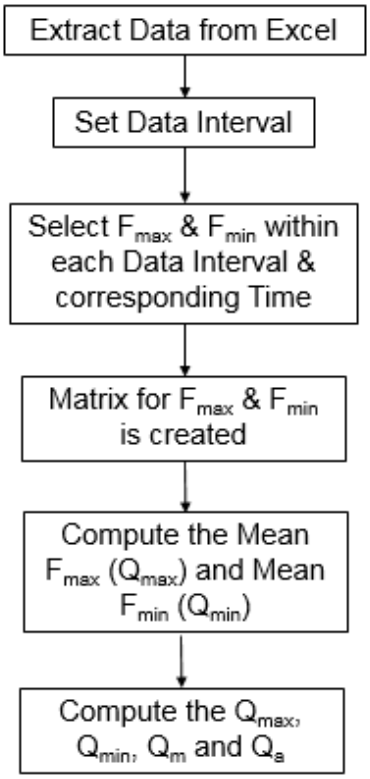

Figure 23. Data filtering algorithm.

1. Data Representation

With the data acquisition rate of 0.025 sec/data point captured by the MTS built-in software, a massive pool of data is collected for each composite sample tested. The data collected can be analyzed by plotting the maximum force and minimum force with respect to the fatigue cycle of the sample. Figure 24 shows

the plot of the first ten cycles of the composite sample, and the maximum and minimum force is selected in each data interval.

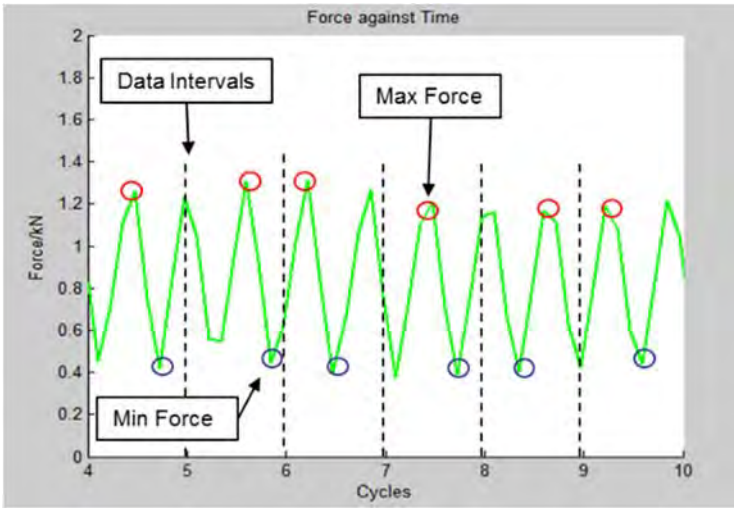

Figure 24. Data acquisition of the maximum and minimum force.

Due to the massive amount of data collected for each experiment, a MATLAB program is written to filter the data by varying the data interval cycles as shown in the Appendix. A pictorial representation of the fatigue life cycle curve with and without data filtering is shown in Figure 25.

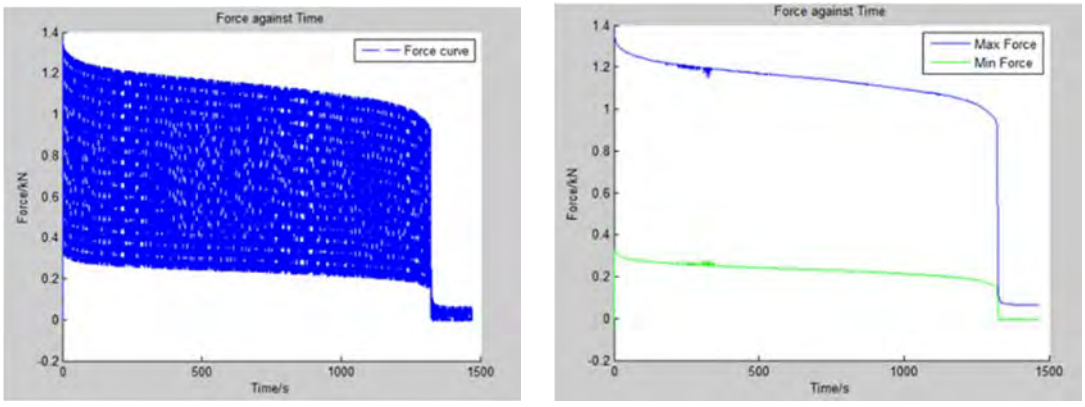

(a) (b)

Figure 25. Fatigue cycle load with (a) no filtering (b) with filtering of 40 cycles per data interval.

The stress-time relationship of the fatigue cyclic curve illustrates a fluctuating stress pattern where the minimum stress and mean stress do not pass through zero. Under fluctuating cyclic loading, it is evident that other than the maximum and minimum stress, the mean stress and mean amplitude are also important parameters that are often used to compare the fatigue strength of materials. In the modified Goodman diagram, the maximum and minimum stress is plotted against the mean stress to define the criterion of fatigue failure of materials [27].

To further analyze the data, the mean of the maximum force and minimum force are calculated and denoted as Q_{max} and Q_{min} respectively. The mean and amplitude of the mean maximum force and mean minimum force are known as Q_m and $Q_{A,}$ shown in Figure 26. The ratio of Q_{max} and Q_{min} is also computed and denoted as the R-ratio. The mean Q_m is used as the baseline parameter to compare the samples between the air and the water submerged conditions.

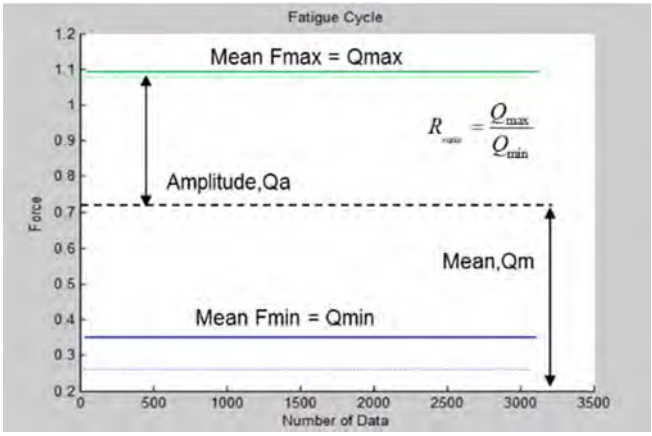

Figure 26. Terminology of data representation.

Multiple samples have been performed for each loading condition to ensure repeatability of the testing data. For the initial discussion, the test specimen for the fifth set of composite samples is discussed. To compare the cyclic loading between air and water submerged conditions, a representative sample of each loading condition is chosen for the comparison study.

2. Fatigue Cyclic Loading at 10 Hz

This section analyzes the results of the composite under fatigue cyclic loading of 10 Hz in air and water submerged conditions. The fatigue failure pattern of the 10 Hz cyclic loading in air and in water submerged loading will be discussed follow by a comparison study between the two medium (air and water). To ensure a baseline comparison between the failure pattern of cyclic loading in air and water, a representative sample with the same average mean force, Q_m, is chosen for the comparison study.

a. Air Loading

The fatigue life cycle of the 10 Hz air loading is summarized in Table 7. The values of the Q_m and Q_a are consistent for all the samples and only a slight variation in the fatigue life cycle was observed. The observation could be due to the scattering of data collected and the nature of the experiment.

Table 7. Summary of 10 Hz air loading for Batch 5.

Sample	Weight (g)	Fatigue Cycle	R-ratio	Q_m (kN)	Q_a (kN)	Q_{max} (kN)	Q_{min} (kN)
5.8	72.1	9500	4.10	0.69	0.421	1.11	0.27
5.9	72.3	14000	4.07	0.69	0.416	1.10	0.27
5.13	72.7	11000	4.03	0.68	0.415	1.09	0.26

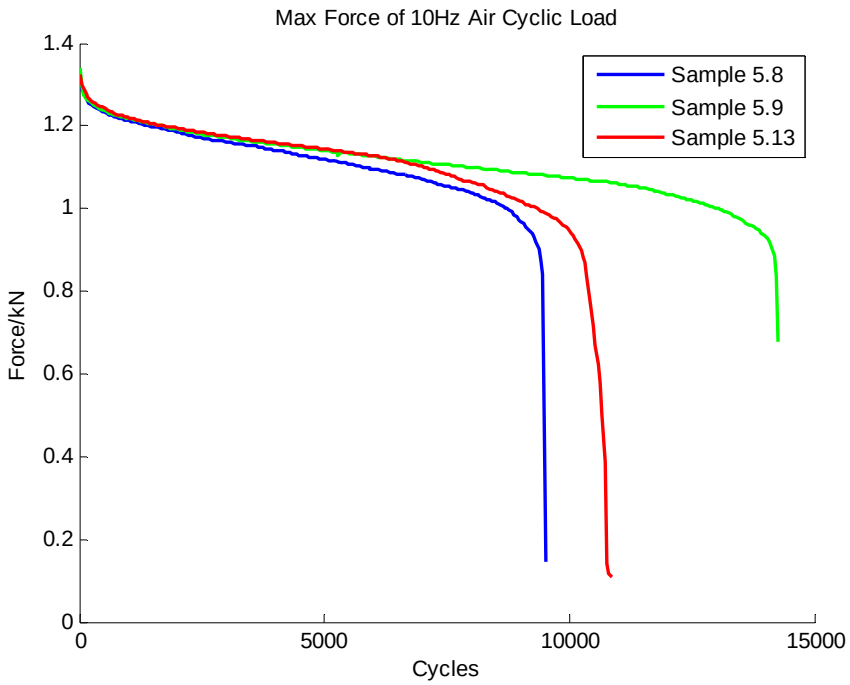

Figure 27. Max. force of 10 Hz air cyclic load for Samples 5.8, 5.9, and 5.13.

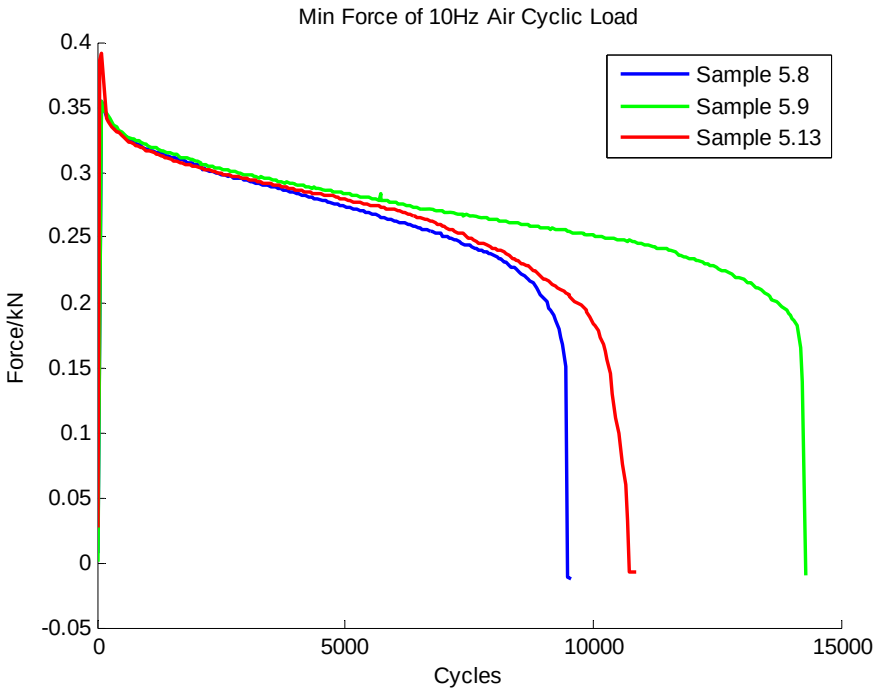

Figure 28. Min. force of 10 Hz air cyclic load for Samples 5.8, 5.9, and 5.13.

The fatigue failure pattern of the composite shows a consistent trend for all the samples under constant cyclic loading of 10 Hz in air. The fatigue strength of the sample decreases rapidly at the initial loading cycles with signs of initial delamination observed in Figure 34. After the initial rapid decrease in strength, the composite exhibits progressive fatigue damage and fails abruptly at 0.9 kN.

b. Water Submerged Loading

The fatigue life cycle of the sample submerged in water exhibits a slight inconsistency in the mean force and amplitude of the fatigue strength of the composite samples. The slight difference in strength of the samples can be due to the difference in weight, dimensions, and stiffness of the individual samples tested.

Table 8. Summary of 10 Hz water loading for Batch 5.

Sample	Weight (g)	Fatigue Cycle	R-ratio	Q_m (kN)	Q_a (kN)	Q_{max} (kN)	Q_{min} (kN)
5.3	72.6	6200	4.37	0.67	0.41	1.08	0.26
5.6	74.5	6900	4.00	0.76	0.46	1.21	0.30
5.7	74.2	5100	3.98	0.78	0.47	1.24	0.31

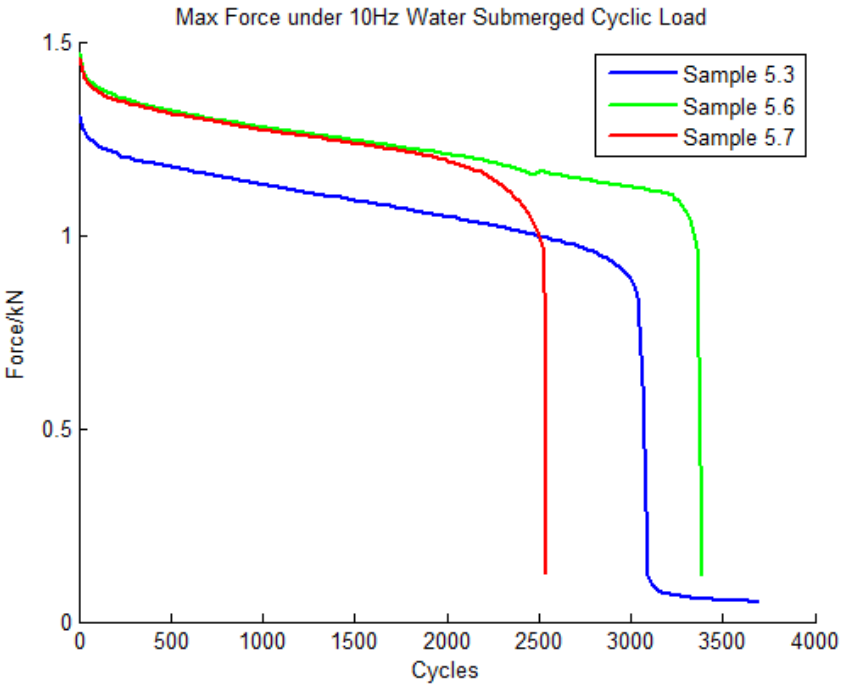

Figure 29. Max. force of 10 Hz water cyclic load for Samples 5.3, 5.6, and 5.7.

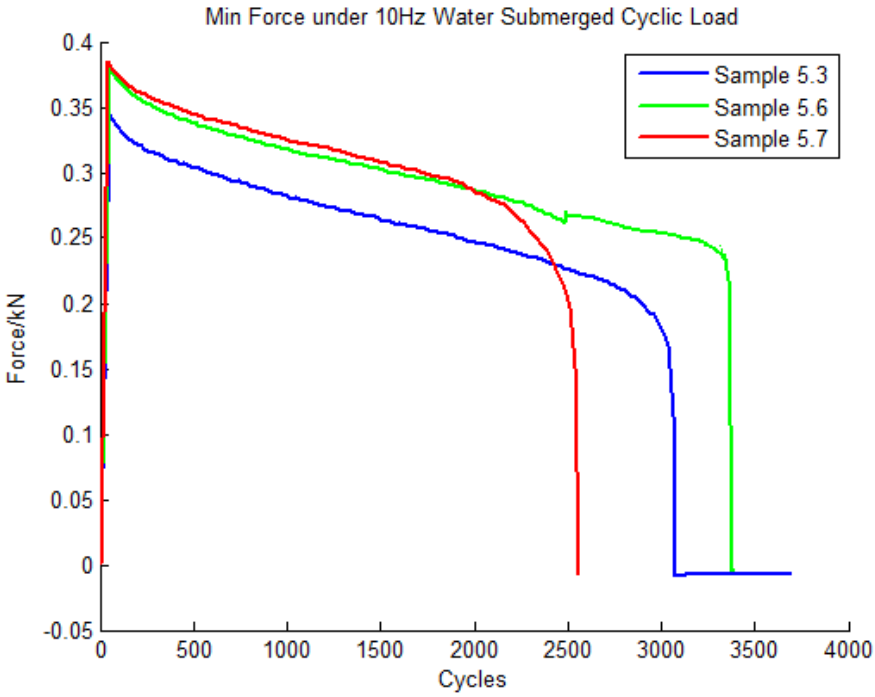

Figure 30. Min. force of 10 Hz water cyclic load for Samples 5.3, 5.6, and 5.7.

The fatigue failure pattern of all the composites under cyclic load in water follows a similar trend displayed in Figure 29 and Figure 30. The fatigue strength of the composite fails rapidly at the initial loading cycles. Thereafter, a progressive and gradual decrease in fatigue strength is observed. The failure force of the composite varies among the composite samples. This could be due to the differences in the average mean force, Q_m, of the composite. As composite Sample 5.6 and Sample 5.7 have the same Q_m, the point of failure for the two samples is approximately 1.1 kN while sample 5.3 fails at 0.8 kN.

c. Comparing Air and Submerged Loading for 10 Hz

To do a comparison study between the air and water submerged loading, a representative sample from each loading condition is chosen with the same average mean force, Q_m. Sample 5.13 and Sample 5.3 were chosen representing the air and water submerged loading, respectively (Figure 31).

Table 9 shows the comparison data between the air and water submerged loading for 10 Hz. With the same Q_m as the base line, the fatigue life cycle for air loading is significantly higher than the life cycle for the loading under water submerged condition. The air-to-water ratio is approximately 1.77. The fatigue failure for both air and water submerged conditions follows the same tread, as shown in Figure 32 and Figure 33.

Table 9. Comparing air and water submerged loading for 10 Hz.

Condition	Sample	Weight (g)	Fatigue Cycle	R ratio	Q_m (kN)	Q_a (kN)	Q_{max} (kN)	Q_{min} (kN)
Air	5.13	72.7	11000	4.03	0.68	0.415	1.09	0.26
Water	5.3	72.6	6200	4.10	0.67	0.410	1.08	0.26

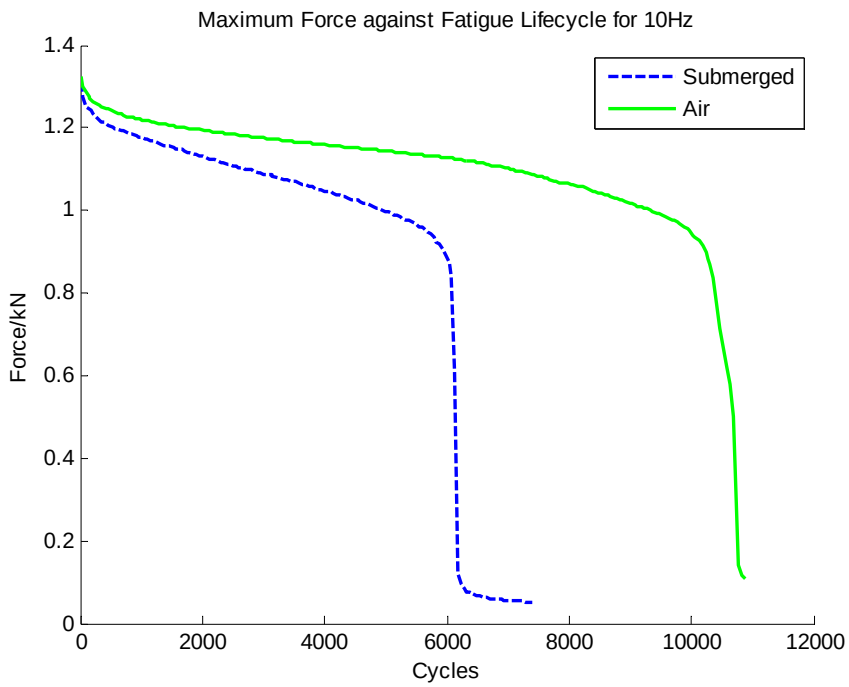

Figure 31. Max. force against fatigue life cycle for 10 Hz loading in air and water submerged conditions.

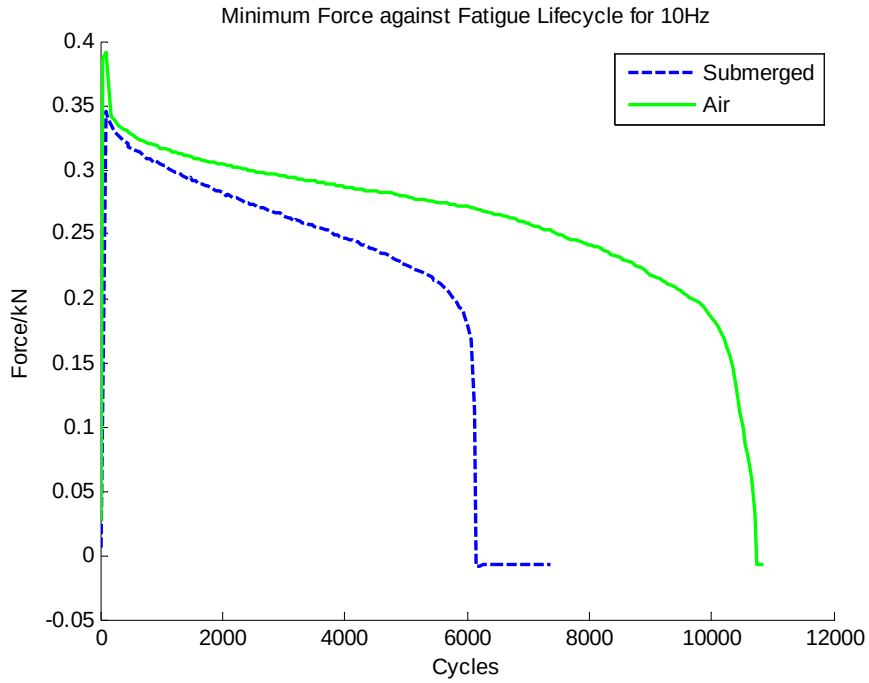

Figure 32. Min. force against fatigue life cycle for 10 Hz loading in air and water submerged conditions.

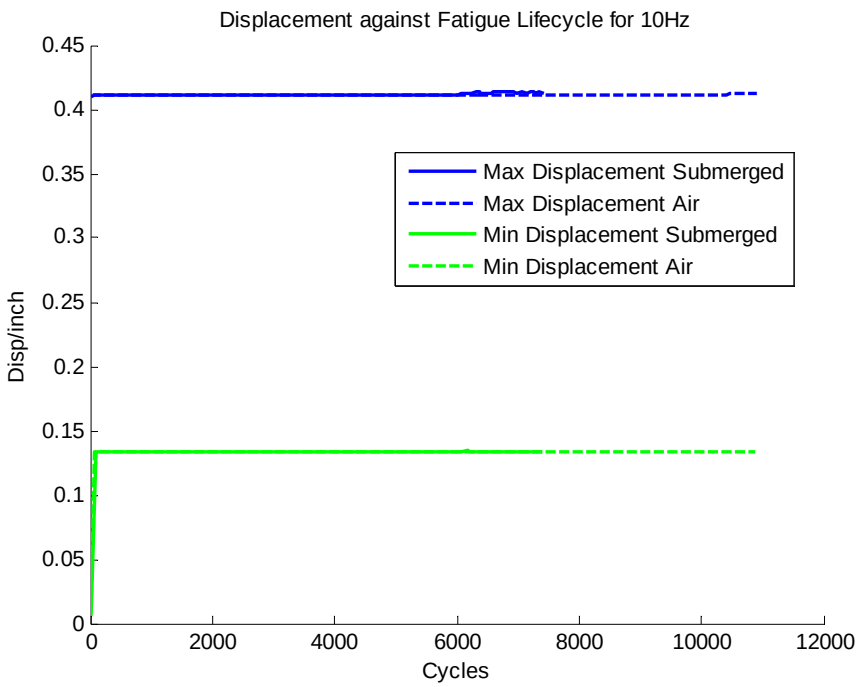

Figure 33. Max. and Min. displacement against fatigue life cycle for 10 Hz loading in air and water submerged conditions.

There is a rapid decrease in fatigue strength for both samples at the first 500 life cycles, and delamination at the initial loading cycles was observed, as shown in Figure 34. The microcrack on the surface of the impact is described to distribute the stress concentration and prolong the initial life cycle of the composite [16]. The rapid decrease in fatigue strength at the initial loading can be attributed to the damage of the fiber matrix at high load. However, since the reinforcing fiber matrix is not damaged, the initial delamination does not affect the bulk strength of the composite sample.

After the first 500 life cycles, both samples exhibit a progressive and gradual failure rate. However, the gradient of fatigue failure for the water submerged sample is significantly steeper than the sample with air loading. The increase in the rate of fatigue failure for water submerged loading can be due to the influence of FSI with the “added mass” effect that impacts the structure.

It was observed that both samples failed at 0.9 kN. This shows that the mechanical properties of the composite are unlikely to be affected by moisture which weakens the structure. The displacement curve in Figure 33 shows that the same displacement loading has been applied to both samples throughout the experiment.

(a) (b)

Figure 34. Signs of delamination of sample after initial loading in (a) air load (b) submerged water loading.

3. Fatigue Cyclic Loading at 5 Hz

This section analyzes the results of the composite under fatigue cyclic loading of 5 Hz in air and water submerged conditions. The fatigue failure pattern of the 5 Hz cyclic loading in air and in water submerged loading will be discussed follow by a comparison study between the two medium (air and water). To ensure a baseline comparison between the failure pattern of cyclic loading in air and water, a representative sample with the same average mean force, Q_m, is chosen for the comparison study.

a. Air Loading

The fatigue life cycle of the 5Hz air loading is summarized in Table 10. The values of the Q_m and Q_a are consistent for all the samples and only a slight variation in the fatigue life cycle was observed.

The fatigue failure of the 5 Hz cyclic load in air shows a similar trend for all the composite samples in Figure 35 and Figure 36. An initial rapid decrease in fatigue strength was observed for the first 500 cycles, followed by a progressive and gradual decrease in fatigue strength. The samples fractured and failed at the range of 1.0 to 1.15 kN.

Table 10. Summary of 5 Hz air loading for Batch 5.

Sample	Weight (g)	Fatigue Cycle	R-ratio	Q_m (kN)	Q_a (kN)	Q_{max} (kN)	Q_{min} (kN)
5.10	71.7	6000	3.73	0.75	0.43	1.18	0.32
5.11	72.9	8900	3.94	0.73	0.43	1.16	0.30
5.14	72.3	5800	3.53	0.76	0.43	1.19	0.34

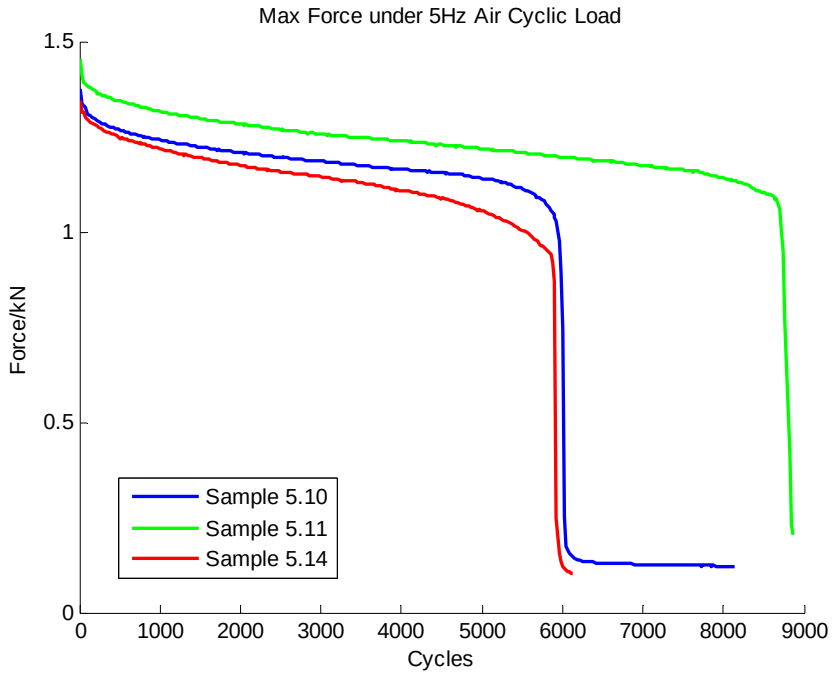

Figure 35. Max. force of 5 Hz air cyclic load for Samples 5.10, 5.11, and 5.14.

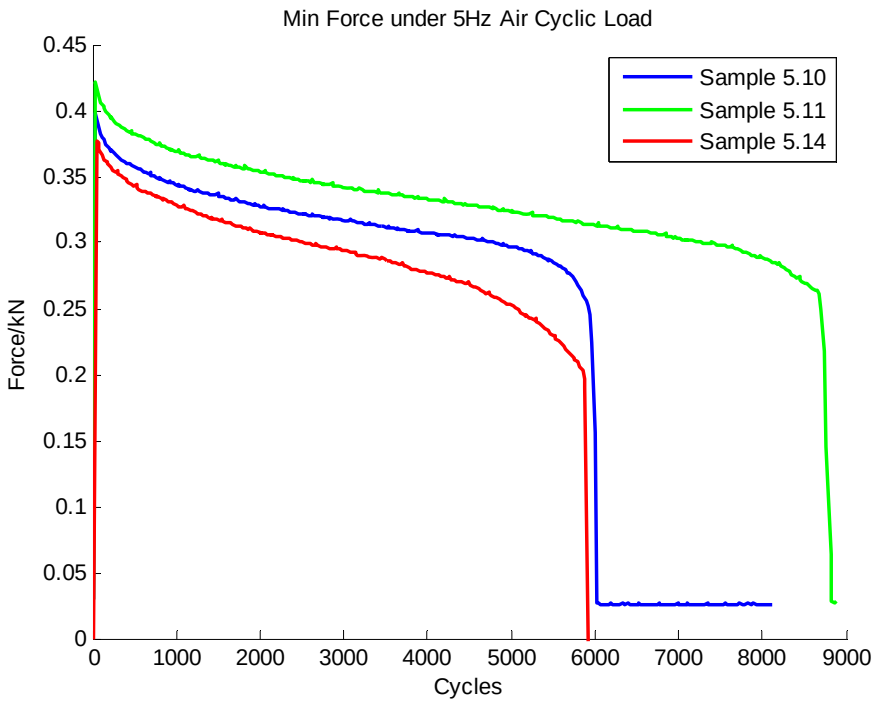

Figure 36. Min. force of 5 Hz air cyclic load for Samples 5.10, 5.11, and 5.14.

b. Water Submerged Loading

The fatigue life cycle of the 5 Hz water loading is summarized in Table 11. The values of the fatigue life cycle, Q_m and Q_a, are consistent for Samples 5.4 and 5.5, but Sample 5.16 shows a slight variation in the strength of the composite. This could be due to the difference in the physical dimensions of the sample as the weight of Sample 5.16 is significantly larger than Samples 5.4 and 5.5.

The fatigue deformation of all the composites follows a similar trend with an initial rapid fatigue failure at the first 500 cycles, followed by a progressive decrease in fatigue strength. The samples fractured at the range of 1.0 to 1.2 kN.

Table 11. Summary of 5 Hz water loading for Batch 5.

Sample	Weight (g)	Fatigue Cycle	R-ratio	Q_m (kN)	Q_a (kN)	Q_{max} (kN)	Q_{min} (kN)
5.4	73.4	3500	3.85	0.75	0.44	1.19	0.31
5.5	73.5	3400	3.86	0.76	0.45	1.21	0.31
5.16	77.3	3700	4.26	0.71	0.44	1.15	0.27

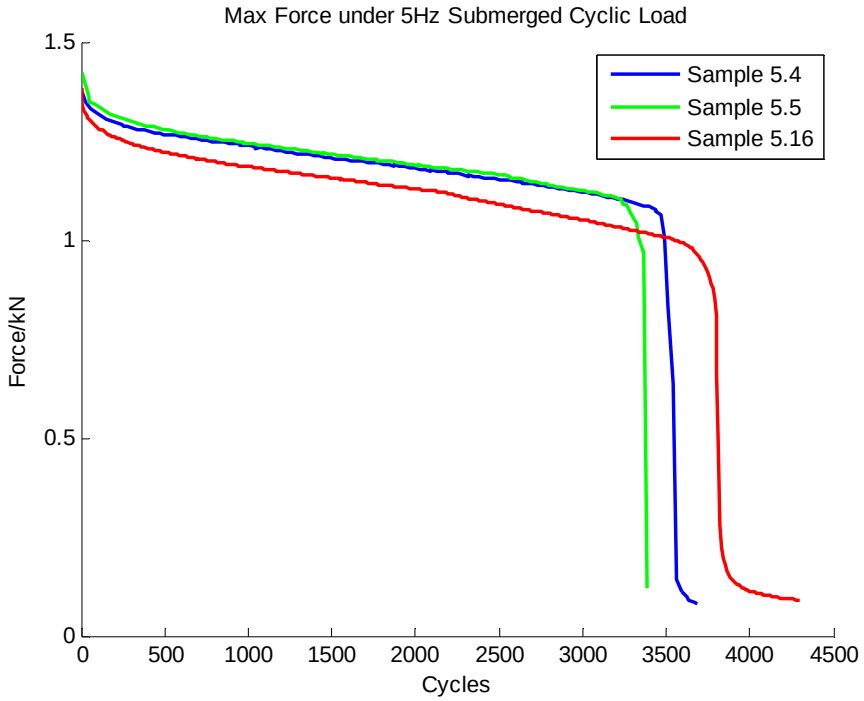

Figure 37. Max. force of 5 Hz water cyclic load for Samples 5.4, 5.5, and 5.16.

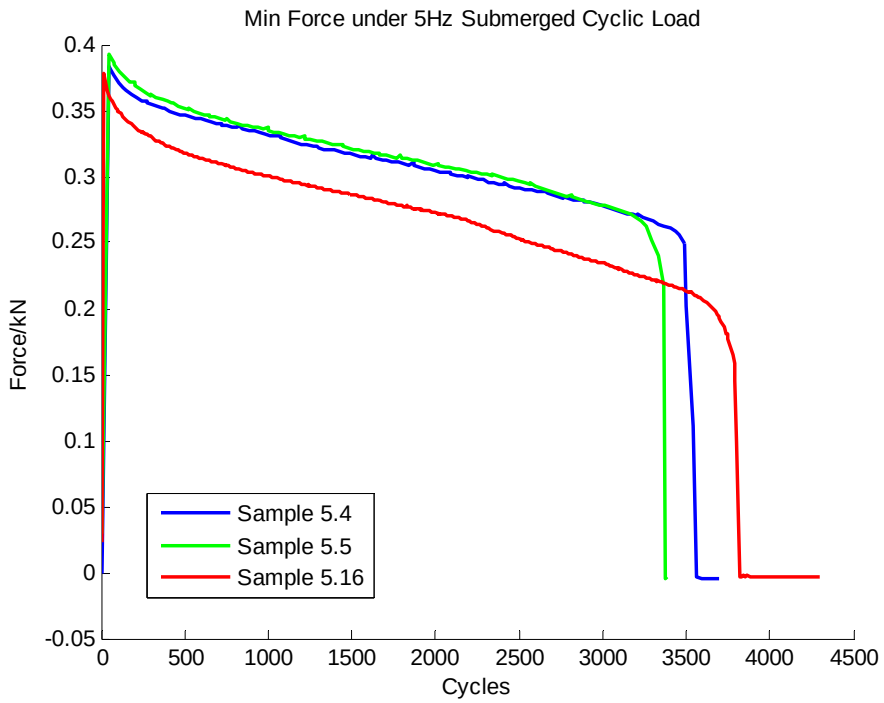

Figure 38. Min. force of 5 Hz water cyclic load for samples 5.4, 5.5, and 5.16.

c. Comparing Air and Submerged Loading for 5Hz

To ensure that there is a baseline comparison for the air and water submerged condition, a representative sample of the same average mean force, Q_m, is selected for comparison. Sample 5.10 and Sample 5.4 reflect the fatigue cyclic load for air and submerged conditions, respectively, as shown in Table 12.

Table 12. Comparing air and submerged loading for 5 Hz.

Condition	Sample	Weight (g)	Fatigue Cycle	R-ratio	Q_m (kN)	Q_a (kN)	Q_{max} (kN)	Q_{min} (kN)
Air	5.10	72.9	6000	3.73	0.75	0.415	1.18	0.32
Water	5.4	73.4	3500	3.85	0.75	0.410	1.19	0.31

Both samples displayed a similar fatigue failure pattern with a rapid decrease in fatigue strength at the initial 500 cycles, displayed in Figure 39 and Figure 40. After 500 cycles, a progressive damage fatigue failure is observed. The gradient of fatigue damage is significantly steeper for the sample in the water submerged condition when compared to the air loading. FSI can be observed with the difference in fatigue failure rate between the two loading conditions. A higher fatigue failure rate at the progressive damage region was observed. This could be due to the “added mass” effect which increases the impact force exerted on the composite sample. The fatigue life cycle ratio between air and submerged water loading is 1.71.

The fatigue failure for both samples occurred at approximately 1.05 kN. This shows that the mechanical strength of both samples exhibits the same characteristics and the fatigue strength of Sample 5.4 under water submerged conditions was not affected by moisture absorption during the experiment. Figure 41 shows that the displacement loading was constant for both samples.

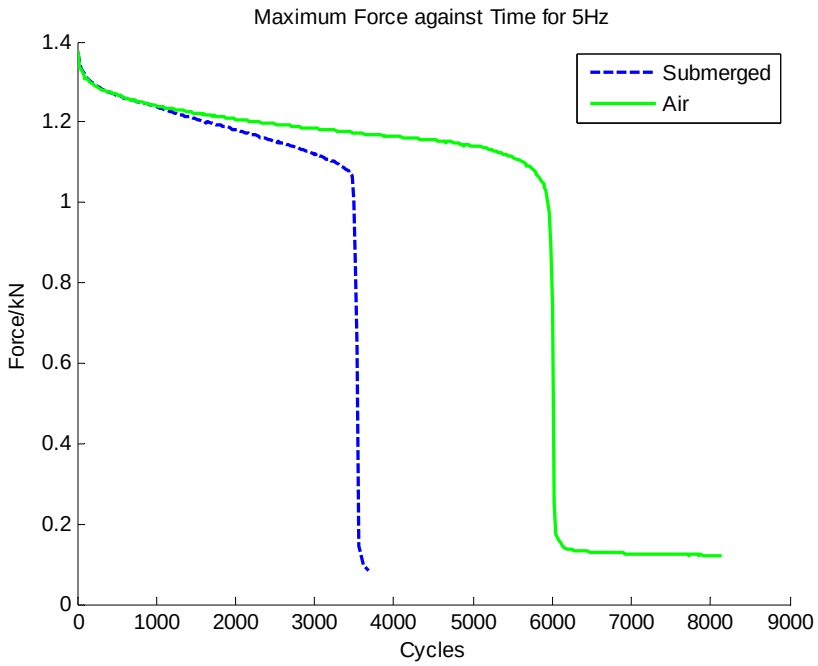

Figure 39. Max. force against fatigue life cycle for 5 Hz loading in air and water submerged conditions.

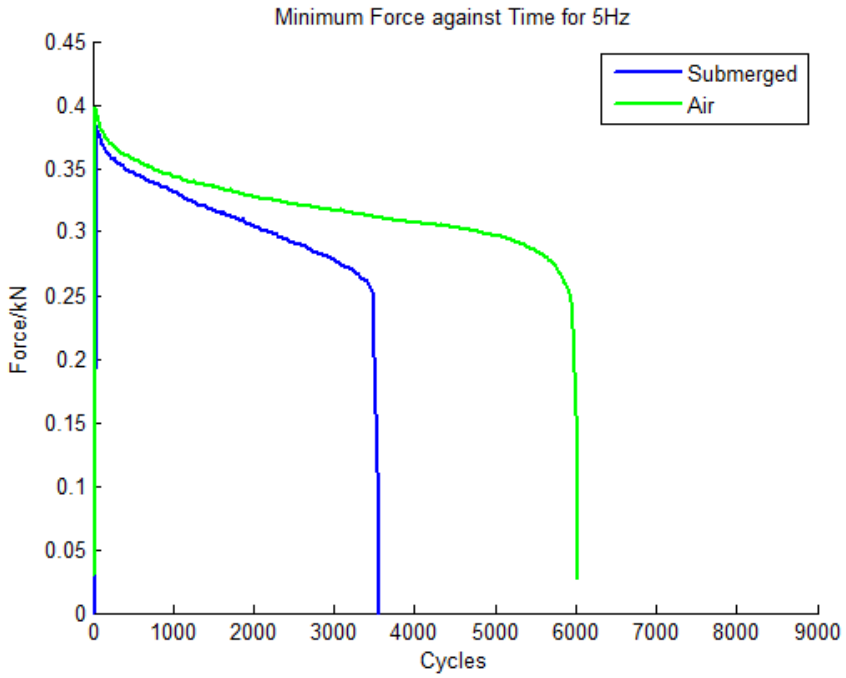

Figure 40. Min. force against fatigue life cycle for 5 Hz loading in air and water submerged conditions.

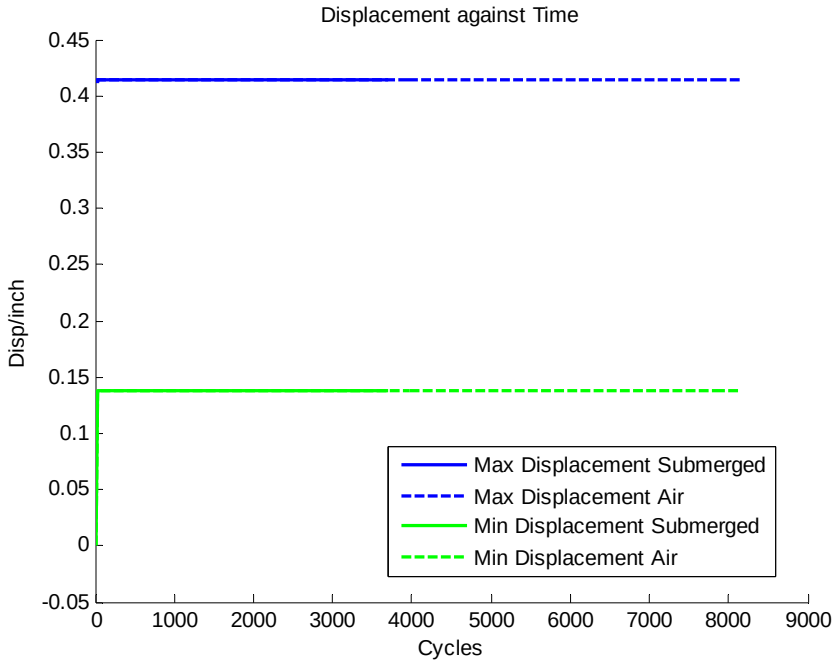

Figure 41. Max. and Min. displacement against fatigue life cycle for 5Hz loading in air and water submerged conditions.

4. Fatigue Cyclic Loading of 2Hz

This section analyzes the results of the composite under fatigue cyclic loading of 2 Hz in air and water submerged conditions. The fatigue failure pattern of the 2 Hz cyclic loading in air and in water submerged loading will be discussed follow by a comparison study between the two medium (air and water). To ensure a baseline comparison between the failure pattern of cyclic loading in air and water, a representative sample with the same average mean force, $Q_{m,}$ chosen for the comparison study.

a. Air Loading

The fatigue life cycle of the 2 Hz air loading is summarized in Table 13. Due to the limitation of the number of samples, only two samples were chosen for the experiment. Comparing the two samples, a large variation was observed with significant difference in the life cycle, Q_m and Q_a, of the experiment. Sample 5.12 is suspected to have slipped during the experiment due to the low fatigue force at the onset of the experiment. The fatigue failure of 2 Hz air loading follows a similar trend as the rest of the samples with an initial rapid decrease in fatigue strength and followed by a progressively damaged region shown in Figure 42 and Figure 43.

Table 13. Summary of fatigue cycle under 2 Hz air loading.

Sample	Weight (g)	Fatigue Cycle	R-ratio	Q_m (kN)	Q_a (kN)	Q_{max} (kN)	Q_{min} (kN)
5.12	73.4	36000	4.20	0.54	0,36	0.9	0.19
5.20	73.4	12500	3.98	0.78	0.47	1.25	0.31

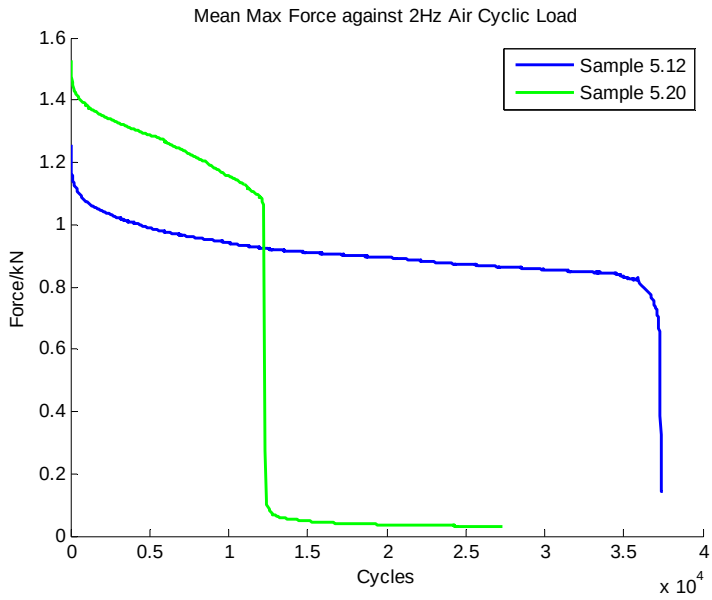

Figure 42. Max. force of 2 Hz in air cyclic loading for sample 5.12 and 5.20.

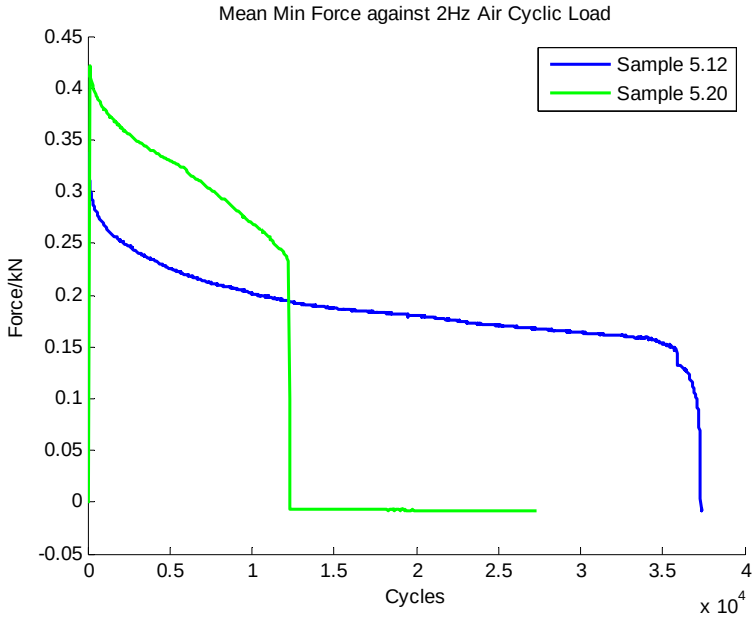

Figure 43. Min. force of 2 Hz air cyclic loading for sample 5.12 and 5.20.

b. Water Submerged Loading

The fatigue life cycle of 2 Hz water loading is summarized in Table 14. Due to the limitation of the number of samples available, only two samples were allocated for the experiment. The samples show only a slight variation in the average mean force, Q_m, and fatigue life cycle of the two composite samples.

Table 14. Summary of fatigue cycle under 2 Hz water loading.

Sample	Weight (g)	Fatigue Cycle	R-ratio	Q_m (kN)	Q_a (kN)	Q_{max} (kN)	Q_{min} (kN)
5.17	73.4	12000	3.85	0.67	0.507	1.18	0.17
5.18	73.5	13000	3.86	0.60	0.502	1.11	0.10

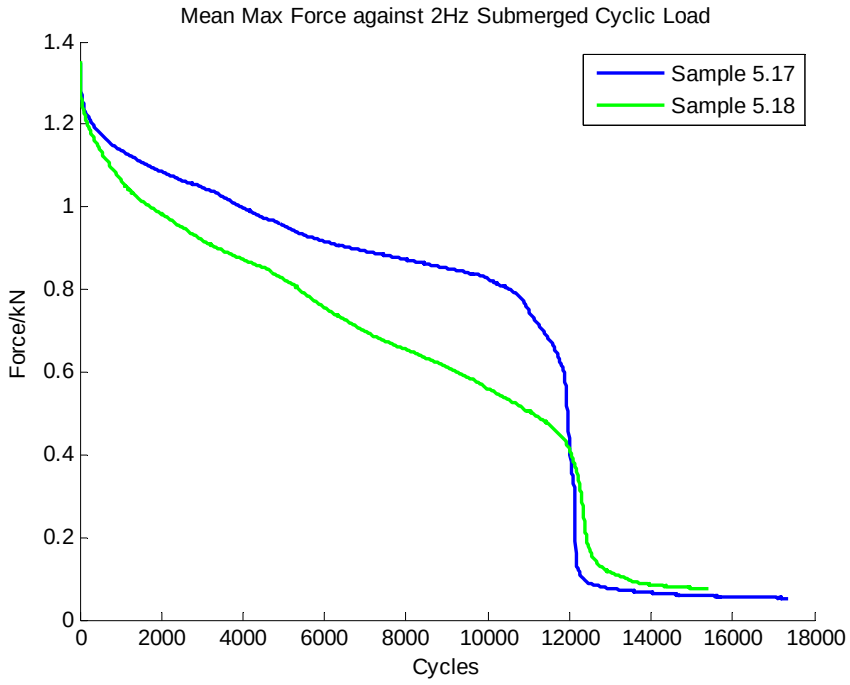

Figure 44. Max. force of 2 Hz water cyclic loading for sample 5.17 and 5.18.

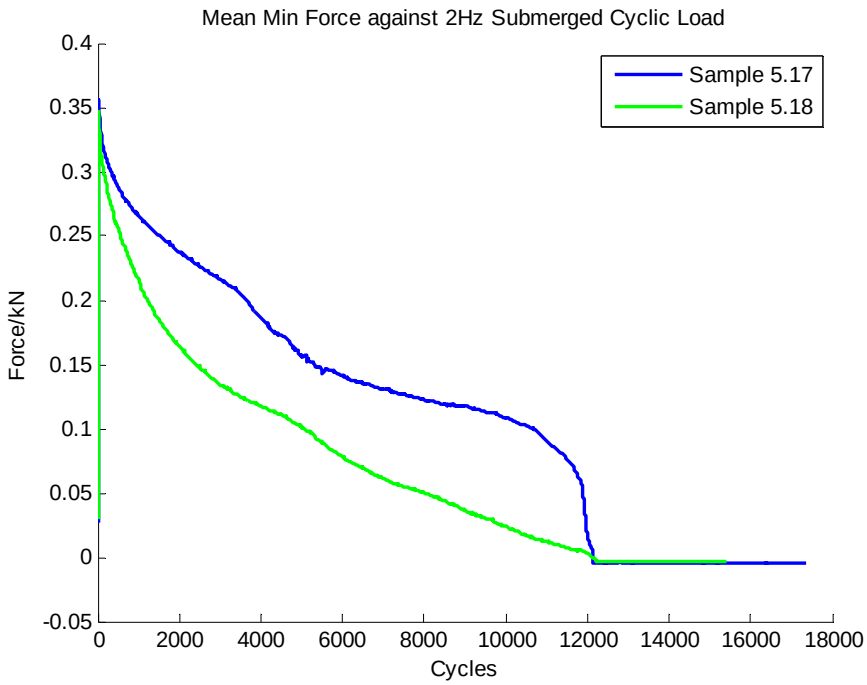

Figure 45. Min. force of 2 Hz water cyclic loading for sample 5.17 and 5.18.

c. Comparing Air and Water Submerged Loading for 2 Hz

To ensure that there is a baseline comparison for the air and water submerged conditions, a representative sample of the same average mean force, Q_m, should be selected. However, due to the limitation of the samples tested for the 2 Hz cyclic loading test, two samples of the same Q_m cannot be found. As such, the comparison study was done choosing samples with the closest mean force, Q_m. Sample 5.20 and Sample 5.17 were chosen and they depict the fatigue cyclic loading for air and water submerged conditions, respectively.

Table 15. Comparing air and water submerged loading for 2 Hz.

Condition	Sample	Weight (g)	Fatigue Cycle	R ratio	Q_m (kN)	Q_a (kN)	Q_{max} (kN)	Q_{min} (kN)
Air	5.20	73.4	12500	3.98	0.78	0.469	1.25	0.315
Water	5.17	73.4	12000	7.12	0.67	0.507	1.18	0.166

Both samples display similar fatigue failure patterns with a rapid decrease in fatigue strength at the initial 500 cycles as shown in Figure 46 and Figure 47. After 500 cycles, a progressive damage fatigue failure is observed. The gradient of fatigue damage for the force is only slightly steeper for the sample with the water submerged condition when compared to the air loading. Although FSI can be observed with the difference in fatigue failure rates between the two conditions, the degree of difference is not significant. The fatigue life cycle ratio between air and submerged water loading is 1.04.

The failure force for both samples is different because the average mean force, Q_m, for both samples is not the same. Figure 48 shows that the displacement loading for both samples have the same throughout the experiment.

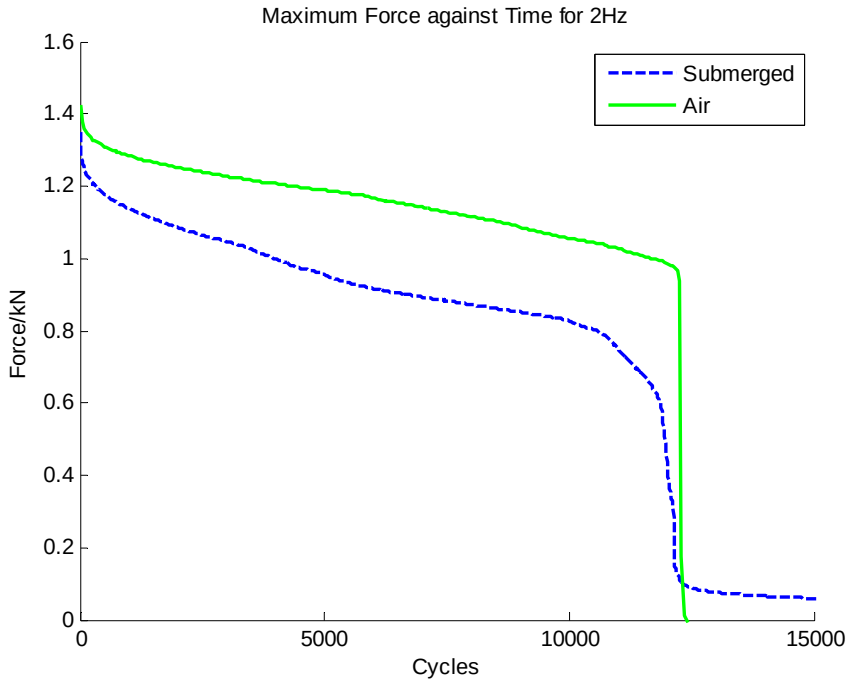

Figure 46. Max. force against fatigue life cycle for 2 Hz loading in air and water submerged conditions.

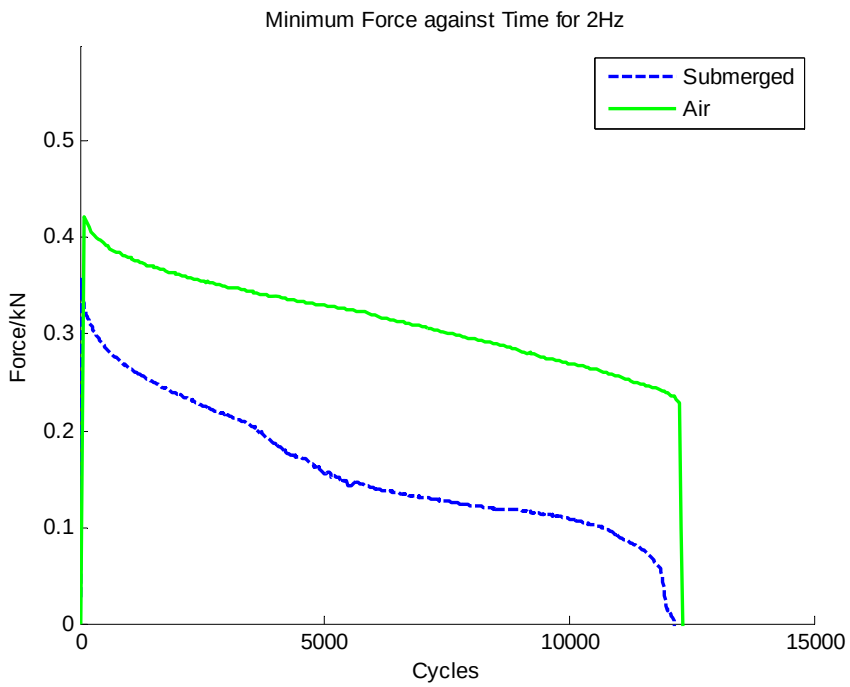

Figure 47. Min. force against fatigue life cycle for 2 Hz loading in air and water submerged conditions.

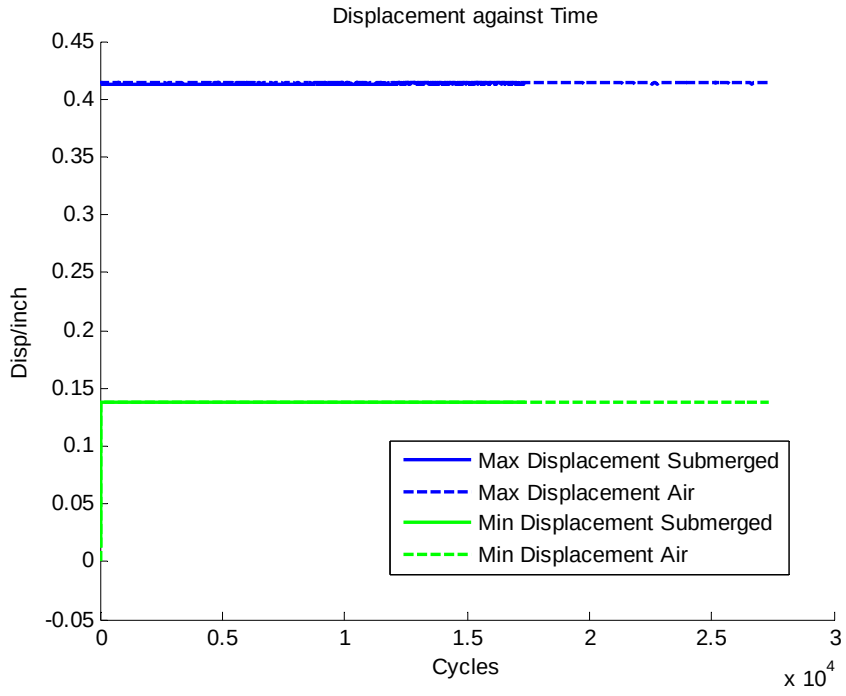

Figure 48. Max. and Min. Displacement against fatigue life cycle for 2 Hz loading in air and water submerged conditions.

5. Comparing Fatigue Cyclic Failure for 10 Hz, 5 Hz, and 2 Hz

Table 16 summaries the comparison data for Batch 5 composites with the fatigue cyclic loading of 10 Hz, 5 Hz and 2 Hz in air and water submerged conditions. The effect of FSI can be observed from the air-to-water ratio of the fatigue life cycle. From the table, the fatigue life cycle of the air-to-water ratio is significantly higher in high frequency loading of 10 Hz to 5 Hz when compared to the low frequency loading of 2 Hz.

To ensure consistency in the data collected, a similar comparison study was done for the rest of the composite batches fabricated and the results are shown in Table 17, Table 18, Table 19, and Table 20. The data tabulated in Table 21 summarizes all the air-to-water ratios of the fatigue life cycle of the composites fabricated for the comparison study. The results from the other composite batches affirm the observation that the FSI effect is more prominent in high frequency loading of 10 Hz and 5 Hz while the low frequency loading of 2 Hz has a less significant effect.

The observation of FSI being less significant in low frequency loading is due to the decrease in “added mass” effect. Under low frequency loading, the inertial force impacting the composite structure is reduced due to the decrease in loading speed on the composite. The decrease in inertial force impacting the composite structure reduces the FSI effect.

Table 16. Comparing fatigue cyclic failure for 10 Hz, 5H z, and 2 Hz of Batch 5 samples.

Composite Fabricated: Batch 5 **Stiffness: 122.9 kN/m** **Loading Condition : 10.5mm (Max Disp) and 3.5mm (Min Disp)**						
Frequency	**2Hz**		**5Hz**		**10Hz**	
	Air	Water	Air	Water	Air	Water
Sample	5.20	5.17	5.10	5.4	5.13	5.3
Q_m	0.78	0.67	0.75	0.75	0.68	0.67
Q_a	0.47	0.51	0.43	0.44	0.42	0.41
Life cycle	12000	12500	6000	3500	11000	6200
Air-to-Water Ratio	**1.04**		**1.71**		**1.77**	

Table 17. Comparing fatigue cyclic failure for 10 Hz, 5 Hz, and 2 Hz of Batch 6 samples.

Composite Fabricated: Batch 6 **Stiffness: 138 kN/m** **Loading Condition : 9.3 mm (Max Disp) and 3.1 mm (Min Disp)**						
Frequency	**2Hz**		**5Hz**		**10Hz**	
	Air	Water	Air	Water	Air	Water
Sample	6.5	6.8	6.4	6.13	6.3	6.14
Q_m	0.64	0.51	0.64	0.59	0.65	0.67
Q_a	0.39	0.37	0.39	0.35	0.40	0.42
Life cycle	30000	27000	29000	21000	31000	24000
Air-to-Water Ratio	**1.11**		**1.38**		**1.29**	

Table 18. Comparing fatigue cyclic failure for 10 Hz,and 5 Hz of Batch 4 samples.

Composite Fabricated: Batch 4 **Stiffness: 135.8 kN/m** **Loading Condition : 9.6 mm (Max Disp) and 3.2mm (Min Disp)**				
Frequency	**5Hz**		**10Hz**	
Parameter	Air	Water	Air	Water
Sample	4.13	4.18	4.14	4.8
Q_m	0.72	0.72	0.70	0.71
Q_a	0.44	0.43	0.43	0.42
Life cycle	11500	8000	25000	18000
Air-to-Water Ratio	**1.44**		**1.39**	

Table 19. Comparing fatigue cyclic failure for 10 Hz of Batch 3 samples.

Composite Fabricated: Batch 3 **Stiffness: 97.8 kN/m** **Loading Condition : 12 mm (Max Disp) and 4 mm (Min Disp)**					
Frequency	**10Hz**				
Parameter	Sample	Q_m	Q_a	Life cycle	Air to Water Ratio
Air	3.7	0.748	0.436	3000	1.2
Water	3.5	0.744	0.4	1800	

Table 20. Comparing fatigue cyclic failure for 10 Hz of Batch 2 samples.

Composite Fabricated: Batch 2 **Stiffness: 142.8 kN/m** **Loading Condition : 10 mm (Max Disp) and 3.35 mm (Min Disp)**					
Frequency	**10Hz**				
Parameter	Sample	Q_m	Q_a	Life cycle	Air to Water Ratio
Air	2.8	0.617	0.44	27000	1.5
Water	2.5	0.54	0.42	18000	

Table 21. Summary of the air-to-water ratio of all the composites fabricated.

Batch	Stiffness (kN/m)	Fatigue Cycle of Air-to-Water Ratio		
		10Hz	5Hz	2Hz
2	142.8	1.50		
3	97.8	1.20		
4	125.8	1.39	1.48	
5	122.9	1.77	1.7	1.04
6	138.1	1.29	1.38	1.11

V. CONCLUSION

The objective of the study was to investigate the effects of FSI on composites under cyclic loading. Cyclic loading of 10 Hz, 5 Hz, and 2 Hz were performed to determine the effect of FSI with the varied loading conditions. The results of the experiment show that FSI, due to “added mass” effect, significantly affects the composite structure under cyclic loading and the degree of influence is relatively higher in high frequency loading.

According to the experiment data tabulated in Table 21, the degree of FSI on composites varies, but not proportionally, to the stiffness of the composite. On average, the effect of “added mass” due to high frequency loading of 10 Hz and 5 Hz results in a decrease in the fatigue life cycle of the composite samples by 43 percent and 52 percent, respectively. The decrease in fatigue life cycle of the composite samples for the 2 Hz cyclic loading is approximately 7.5 percent. The results show that the effect of FSI due to low frequency loading of 2 Hz is relatively less prominent. The reason for the observation can be due to the decrease in cyclic velocity on the composite sample which reduces the “added mass” effect.

The results of the study affirm the importance of FSI and how it affects the mechanical properties and fatigue strength of composites. Due to the “added mass” effect, composite structures tend to fail earlier in fluid submerged conditions. As such, the FSI effect has to be addressed in ship hull design and construction. Ongoing research is being done to develop future life prediction and modeling tools for submerged structures in fluid. The results from this study provide valuable insights into the fatigue behaviors and failure pattern of composites under vibratory and cyclic loading in a fluid submerged environment.

To refine and improve on this experimental study, the mean displacement between the maximum displacement and the minimum displacement for the cyclic loading condition should be identified as the baseline loading condition for the entire batch of composites tested. This will reduce the variation of data and contribute to a better comparison study. In addition, the loading jig that holds the sample during the experiment should be modified to lightly secure the sides of the sample to prevent the movement of samples during the cycle load.

Future studies can be performed to investigate the degree of FSI for 5 Hz loading. The results from Table 21 show that, on average, the effect of FSI for 5 Hz loading is comparatively higher than for 10 Hz cyclic loading. More experimental research can be performed on varied frequencies of 4Hz to 7Hz to identify any possible trends during the cyclic loading.

APPENDIX

```
% - Build array of time components.
% Extract Data for 10Hz, 5Hz or2Hz

clear all;

load sample_4_2.mat
Data = cell2mat(sample_4_2);
Data = Data(2:end, :);
data_interval=200;
Ind = Data(:,1);
Time = Data(:,2);
Force = Data(:,3);
Disp = Data(:,4);
num_Sets = ((length(Ind))/data_interval);
hz=5;
period=1/hz;
%num_Sets = length(Ind);

% Find maximum in each set
Max_Force = [];
Min_Force = [];
Max_Disp = [];
Min_Disp = [];
CMax_F_Time = [];
CMin_F_Time = [];
CMax_D_Time = [];
CMin_D_Time = [];


for i = 1:num_Sets

    %Find Max Force
    CurrSet_Force = Force((i-1)*data_interval+1 : i*data_interval);
    Max_Force = [Max_Force ; max(CurrSet_Force)];
    Max_Ind_F = find(CurrSet_Force == Max_Force(i)) + ((i-
1)*data_interval);
    if length(Max_Ind_F) > 1
        Max_Ind_F = Max_Ind_F(end);
    end
    CMax_F_Time = [CMax_F_Time ; Time(Max_Ind_F)];

    %Find Min Force
    Min_Force = [Min_Force ; min(CurrSet_Force)];
    Min_Ind_F = find(CurrSet_Force == Min_Force(i)) + ((i-
1)*data_interval);
    if length(Min_Ind_F) > 1
        Min_Ind_F = Min_Ind_F(end);
    end
    CMin_F_Time = [CMin_F_Time ; Time(Min_Ind_F)];
```

```
    % Find Max Displacement
    CurrSet_Disp = Disp((i-1)*data_interval+1 : i*data_interval);
    Max_Disp = [Max_Disp ; max(CurrSet_Disp)];
    Max_Ind_D = find(CurrSet_Disp == Max_Disp(i)) + ((i-
1)*data_interval);
    if length(Max_Ind_D) > 1
        Max_Ind_D = Max_Ind_D(end);
    end
    CMax_D_Time = [CMax_D_Time ; Time(Max_Ind_D)];

    % Find Min Displacement
    Min_Disp = [Min_Disp ; min(CurrSet_Disp)];
    Min_Ind_D = find(CurrSet_Disp == Min_Disp(i)) + ((i-
1)*data_interval);
    if length(Min_Ind_D) > 1
        Min_Ind_D = Min_Ind_D(end);
    end
    CMin_D_Time = [CMin_D_Time ; Time(Min_Ind_D)];
end

Output_Data = [CMax_F_Time, Max_Force,CMin_F_Time, Min_Force,
CMax_D_Time, Max_Disp,CMin_D_Time, Min_Disp];

Time_i=Time(1:data_interval:end);

E=i-1;

Max_Force_1=interp1(CMax_F_Time, Max_Force,Time_i);
Min_Force_1=interp1(CMin_F_Time,Min_Force,Time_i);
R=(Max_Force_1)./(Min_Force_1);

m_Min_Force=mean((Min_Force_1(2:E)))
m_Max_Force=mean(Max_Force_1(2:E))

figure(), hold on;
plot((CMax_F_Time)/period, Max_Force,'b-', (CMin_F_Time)/period,
Min_Force,'g-','LineWidth',2);
title('Force against Time')
xlabel('Cycles')
ylabel('Force/kN')
legend('Max Force', 'in Force');
hold off;

figure(), hold on;
plot((CMax_D_Time)/period, Max_Disp,'b-', (CMin_D_Time)/period,
Min_Disp,'g-','LineWidth',2);
title('Displacement against Time')
xlabel('Cycles')
ylabel('Disp/inch')
legend('Max Displacement', 'in Displacement');
hold off;
```

LIST OF REFERENCES

[1] A. Mouritz, E. Gellert, P. Burchill, and K. Challis, “Review of advanced composite structures for naval ships and submarines,” *Composite Structures*, vol. 53, pp. 21–42, 2001.

[2] P. L. Francis, *Defense Acquisitions: Cost to Deliver Zumwalt-Class Destroyers Likely to Exceed Budget*. Philadelphia, PA: Diane Publishing, 2009.

[3] A. Rosen, K. Garme, and J. Kuttenkeuler, “Full-scale design evaluation of the Visby class corvette,” presented at 9th International Conference on Fast Sea Transportation, Shanghai, China, Sep. 23–27, 2007.

[4] D. McGeorge and B. Høyning, “Fire safety of naval vessels made of composite materials: Fire safety philosophies, ongoing research and state-of-the-art passive fire protection,” presented at NATO RTO Specialists’ Meeting on Fire Safety and Survivability, Aalborg, Denmark, 2002.

[5] C. Brennen, “A review of added mass and fluid inertial forces,” Department of the Navy, Port Hueneme, CA: Caltech Authors, 1982.

[6] R. D. Blevins, *Flow-Induced Vibration*. Malabar, FL: Krieger Publishing, 2001.

[7] M. K. Kwah, “Hydroelastic vibration of rectangular plates,” *J. Appl. Mech.*, vol. 63, pp. 110–115, 1996.

[8] A. C. Owens, “An experimental study of fluid structure interaction of carbon composites under low velocity impact,” M.S. thesis, Mech.Eng, Naval Postgraduate School, Monterey, CA, 2009.

[9] R. L. Sierakowski and S. K. Chaturvedi, *Dynamic loading and characterization of fiber-reinforced composites*. Hoboken, NJ: Wiley, 1997.

[10] M. A. Violette, “Fluid structure interaction effect on sandwich composite structures,” M.S. thesis, Mech. Eng. Dept., Naval Postgraduate School, Monterey, CA, 2011.

[11] R. P. Conner, “Fluid structure interaction effects on composites under low velocity impact,” M.S. thesis, Mech. Eng. Dept., Naval Postgraduate School, Monterey, CA, 2012.

[12] E. M. Priest, “Free vibration response comparison of composite beams with fluid structure interaction,” M.S. thesis, Mech. Eng. Dept., Naval Postgraduate School, Monterey, CA, 2012.

[13] J. Degrieck and W. Van Paepegem, “Fatigue damage modeling of fibre-reinforced composite materials: Review,” *Appl. Mech*. Rev., vol. 54, pp. 279–300, 2001.

[14] J. J. Cain, N. L. Post, S. W. Case, and J. J. Lesko, “R-ratio effects on glass-reinforced polymer composite life and remaining strength,” *Proc. 16th Int. Conf. Composite Materials*, 2007, p. 1.

[15] G. Caprino and G. Giorleo, “Fatigue lifetime of glass fabric/epoxy composites,” *Composites Part A: Applied Science and Manufacturing*, vol. 30, pp. 299–304, 1999.

[16] S. Abrate, *Impact on Composite Structures*. Cambridge, UK: Cambridge Univ. Press, 2005.

[17] M. Z. Khelifa and H. M. Al-Shukri, “Fatigue study of E-glass fiber reinforced polyester composite under fully reversed loading and spectrum loading,” *Eng. Technol.,* vol. 26, pp. 1210–1224, 2008.

[18] T. Porter, “Compression and compression fatigue testing of composite laminates.” *Boeing Military Airplane*, No. D180-27619-1, Seattle, WA, 1982.

[19] R. M. Jones, *Mechanics of Composite Materials*. Mason, OH: CRC Press, 1998.

[20] S. R. Swanson, *Introduction to Design and Analysis with Advanced Composite Materials*. Hoboken, NJ: Prentice-Hall, 1997.

[21] K. Galanis, “Hull construction with composite materials for ships over 100 m in length,” Ph.D. diss., Cambridge, MA: Massachusetts Institute of Technology, 2002.

[22] P. K. Mallick, *Fiber-Reinforced Composites: Materials, Manufacturing, and Design*. Mason, OH: CRC Press, 1993.

[23] Pro-set. (2005, Aug.). M1002 Resin/237 hardener. [Online]. Accessed Sep. 18, 2014. Available: http://www.prosetepoxy.com /PDF/Custom/M1002-237.pdf.

[24] Composites World. (2014, Jan.). Fabrication methods. [Online]. Accessed Sep. 18, 2014. Available: http://www.compositesworld.com /articles/fabrication-methods.

[25] Technical Univ. Barcelona. (2006, Jan.). MTS 810 & 858 material testing systems. [Online]. Accessed Sep. 18, 2014. Available: http://www.upc.edu/sct/documents_equipament/d_77_id-412.pdf.

[26] W. Thomson, *Theory of Vibration with Applications*. Mason, OH: CRC Press, 1996.

[27] J. E. Shigley, *Mechanical Engineering Design*. New York: McGraw-Hill Education, 1977.

THIS PAGE INTENTIONALLY LEFT BLANK

INITIAL DISTRIBUTION LIST

1. Defense Technical Information Centre
   Ft. Belvoir, Virginia

2. Dudley Knox Library
   Naval Postgraduate School
   Monterey, California